Eur. Phys. J. C (2018) 78:306
https://doi.org/10.1140/epjc/s10052-018-5777-1

THE EUROPEAN PHYSICAL JOURNAL C

Regular Article - Theoretical Physics

B-meson anomalies and Higgs physics in flavored $U(1)'$ model

Ligong Bian[1,2,a], **Hyun Min Lee**[2,b], **Chan Beom Park**[3,4,c]

[1] Department of Physics, Chongqing University, Chongqing 401331, China
[2] Department of Physics, Chung-Ang University, Seoul 06974, Korea
[3] Center for Theoretical Physics of the Universe, Institute for Basic Science (IBS), Daejeon 34051, Korea
[4] School of Physics, Korea Institute for Advanced Study, Seoul 02455, Korea

Received: 29 January 2018 / Accepted: 3 April 2018

Abstract We consider a simple extension of the Standard Model with flavor-dependent $U(1)'$, that has been proposed to explain some of B-meson anomalies recently reported at LHCb. The $U(1)'$ charge is chosen as a linear combination of anomaly-free $B_3 - L_3$ and $L_\mu - L_\tau$. In this model, the flavor structure in the SM is restricted due to flavor-dependent $U(1)'$ charges, in particular, quark mixings are induced by a small vacuum expectation value of the extra Higgs doublet. As a result, it is natural to get sizable flavor-violating Yukawa couplings of heavy Higgs bosons involving the bottom quark. In this article, we focus on the phenomenology of the Higgs sector of the model including extra Higgs doublet and singlet scalars. We impose various bounds on the extended Higgs sector from Higgs and electroweak precision data, B-meson mixings and decays as well as unitarity and stability bounds, then discuss the productions and decays of heavy Higgs bosons at the LHC.

1 Introduction

The observed fermion masses and mixing angles are well parametrized by the Higgs Yukawa couplings in the Standard Model (SM). However, the neutrino masses and mixing angles call for the addition of right-handed (RH) neutrinos or physics beyond the SM and, moreover, the flavor structures of quarks and leptons are not understood yet. As there is no flavor changing neutral current at tree level in the SM due to the GIM mechanism, the observation of flavor violation is an important probe of new physics up to very high energy scales and it can be complementary to direct searches at the LHC. In particular, the violation of lepton flavor universality would be a strong hint at new physics.

Recently, there have been interesting reports on the anomalies in rare semileptonic B-meson decays at LHCb such as R_K [1], R_{K^*} [2–4], P_5' [5,6]. The reported value of $R_K = \mathcal{B}(B \to K\mu^+\mu^-)/\mathcal{B}(B \to Ke^+e^-)$ is

$$R_K = 0.745^{+0.097}_{-0.082}, \quad 1\,\text{GeV}^2 < q^2 < 6\,\text{GeV}^2, \tag{1.1}$$

which deviates from the SM prediction by 2.6σ. On the other hand for vector B-mesons, $R_{K^*} = \mathcal{B}(B \to K^*\mu^+\mu^-)/\mathcal{B}(B \to K^*e^+e^-)$ is

$$\begin{aligned} R_{K^*} &= 0.66^{+0.11}_{-0.07}(\text{stat}) \pm 0.03(\text{syst}), \\ &\quad 0.045\,\text{GeV}^2 < q^2 < 1.1\,\text{GeV}^2, \\ R_{K^*} &= 0.69^{+0.11}_{-0.07}(\text{stat}) \pm 0.05(\text{syst}), \\ &\quad 1.1\,\text{GeV}^2 < q^2 < 6.0\,\text{GeV}^2, \end{aligned} \tag{1.2}$$

which again differs from the SM prediction by 2.1–2.3σ and 2.4–2.5σ, depending on the energy bins. Explaining the B-meson anomalies would require new physics violating the lepton flavor universality at a few 100 GeV up to a few 10 TeV, depending on the coupling strength of new particles to the SM. We also note that there have been interesting anomalies in $B \to D^{(*)}\tau\nu$ decays, the so called $R_{D^{(*)}} = \mathcal{B}(B \to D^{(*)}\tau\nu)/\mathcal{B}(B \to D^{(*)}\ell\nu)$ with $\ell = e$, μ, whose experimental values are deviated from the SM values by more than 2σ [7–11].

Motivated by the B-anomalies $R_{K^{(*)}}$, some of the authors recently proposed a simple extension of the SM with extra $U(1)'$ gauge symmetry with flavor-dependent couplings [12]. The $U(1)'$ symmetry is taken as a linear combination of $U(1)_{L_\mu - L_\tau}$ and $U(1)_{B_3 - L_3}$, which might be a good symmetry at low energy and originated from enhanced gauge symmetries such as in the $U(1)$ clockwork framework [13]. In this model, the quark mixings and neutrino masses/mixings require an extended Higgs sector, which has one extra Higgs doublet and multiple singlet scalars beyond the SM. As

[a] e-mail: ligongbian@gmail.com
[b] e-mail: hminlee@cau.ac.kr
[c] e-mail: cbpark@ibs.re.kr

Published online: 18 April 2018

Table 1 $U(1)'$ charges of fermions and scalars

	q_{3L}	u_{3R}	d_{3R}	ℓ_{2L}	e_{2R}	ν_{2R}	ℓ_{3L}	e_{3R}	ν_{3R}
Q'	$\frac{1}{3}x$	$\frac{1}{3}x$	$\frac{1}{3}x$	y	y	y	$-x-y$	$-x-y$	$-x-y$
	S	H_1	H_2	Φ_1	Φ_2	Φ_3			
Q'	$\frac{1}{3}x$	0	$-\frac{1}{3}x$	$-y$	$x+y$	x			

a result, nonzero off-diagonal components of quark mass matrices are obtained from the vacuum expectation value (VEV) of the extra Higgs doublet and correct electroweak symmetry breaking is ensured by the VEV of one of the singlet scalars.

In this paper, we study the phenomenology of the heavy Higgs bosons in the flavored $U(1)'$ model mentioned above. We first show that the correct flavor structure of the SM is well reproduced in the presence of the VEV of the extra Higgs doublet. In particular, in the case with a small VEV of the extra Higgs doublet or small $\tan\beta$, we find that the heavy Higgs bosons have sizable flavor-violating couplings to the bottom quark and reduced flavor-conserving Yukawa couplings to the top quark such that LHC searches for heavy Higgs bosons can be affected by extra or modified production and decay channels. We also briefly mention the implication of our extended Higgs sector for $R_{D^{(*)}}$ anomalies. We discuss various constraints on the extended Higgs sector from Higgs and electroweak precision data, flavor data such as the B-meson mixings and decays, as well as unitarity and stability bounds. For certain benchmark points that can evade such bounds, we study the productions and decays of the heavy Higgs bosons at the LHC and show distinct features of the model with flavor-violating interactions in the Higgs sector.

This paper is organized as follows. First, we begin with a summary of the $U(1)'$ model with the extended Higgs sector and new interactions. The Higgs spectrum and Yukawa couplings for heavy Higgs bosons are presented in Sect. 3. We then discuss various theoretical and phenomenological constraints on the Higgs sector are studied in Sect. 4, and collider signatures of the heavy Higgs bosons at the LHC are studied in Sect. 5. Finally, conclusions are drawn. There are four appendices dealing with the extended Higgs sector, unitarity bounds, quark Yukawa couplings, and the $U(1)'$ interactions.

2 Flavored $U(1)'$ model

We consider a simple extension of the SM with $U(1)'$, where a new gauge boson Z' couples specifically to heavy flavors. It is taken as a linear combination of $U(1)_{L_\mu - L_\tau}$ and $U(1)_{B_3-L_3}$ with

$$Q' \equiv y(L_\mu - L_\tau) + x(B_3 - L_3)$$

for real parameters x and y [12].[1] Introducing two Higgs doublets $H_{1,2}$ is necessary to have right quark masses and mixings. We add one complex singlet scalar S for a correct vacuum to break electroweak symmetry and $U(1)'$. Moreover, in order to cancel the anomalies, the fermion sector is required to include at least two RH neutrinos ν_{iR} $(i = 2, 3)$. One more RH neutrino ν_{1R} with zero $U(1)'$ charge as well as extra singlet scalars, Φ_a $(a = 1, 2, 3)$, with $U(1)'$ charges of $-y, x+y, x$, respectively, are also necessary for neutrino masses and mixings. As $L_\mu - L_\tau$ is extended to RH neutrinos, $L_\mu - L_\tau$ and $L_2 - L_3$ can be used interchangeably in our model. The $U(1)'$ charge assignments are given in Table 1.

The Lagrangian of the model is given as

$$\mathcal{L} = -\frac{1}{4} Z'_{\mu\nu} Z'^{\mu\nu} - \frac{1}{2}\sin\xi\, Z'_{\mu\nu} B^{\mu\nu} + \mathcal{L}_S + \mathcal{L}_Y \tag{2.1}$$

with

$$\mathcal{L}_S = |D_\mu H_1|^2 + |D_\mu H_2|^2 + |D_\mu S|^2 + \sum_{a=1}^{3} |D_\mu \Phi_a| - V(\phi_i), \tag{2.2}$$

where $Z'_{\mu\nu} = \partial_\mu Z'_\nu - \partial_\nu Z'_\mu$ is the field strength of the $U(1)'$ gauge boson, $\sin\xi$ is the gauge kinetic mixing between $U(1)'$ and SM hypercharge, and $D_\mu \phi_i = (\partial_\mu - i g_{Z'} Q'_{\phi_i} Z'_\mu)\phi_i$ are covariant derivatives. Here Q'_{ϕ_i} is the $U(1)'$ charge of ϕ_i, $g_{Z'}$ is the extra gauge coupling. The scalar potential $V(\phi_i)$ is given by $V = V_1 + V_2$ with

$$\begin{aligned} V_1 = {} & \mu_1^2 |H_1|^2 + \mu_2^2 |H_2|^2 - (\mu S H_1^\dagger H_2 + \text{h.c.}) \\ & + \lambda_1 |H_1|^4 + \lambda_2 |H_2|^4 + 2\lambda_3 |H_1|^2 |H_2|^2 \\ & + 2\lambda_4 (H_1^\dagger H_2)(H_2^\dagger H_1) \\ & + 2|S|^2(\kappa_1 |H_1|^2 + \kappa_2 |H_2|^2) + m_S^2 |S|^2 + \lambda_S |S|^4, \end{aligned} \tag{2.3}$$

$$V_2 = \sum_{a=1}^{3} (\mu_{\Phi_a}^2 |\Phi_i|^2 + \lambda_{\Phi_a} |\Phi_a|^4)$$

[1] We note that we can take two independent parameters for the Z' couplings to be either $(x g_{Z'},\ y g_{Z'})$ or $(x/y,\ g_{Z'})$ by absorbing y into $g_{Z'}$. Our following discussion does not depend on the choice of the Z' couplings.

$$+ (\lambda_{S3} S^3 \Phi_3^\dagger + \mu_4 \Phi_1 \Phi_2 \Phi_3^\dagger + \text{h.c.}) + 2\sum_{a=1}^{3} |\Phi_a|^2 (\beta_{a1}|H_1|^2 + \beta_{a2}|H_2|^2 + \beta_{a3}|S|^2) + 2\sum_{a<b} \lambda_{ab} |\Phi_a|^2 |\Phi_b|^2. \tag{2.4}$$

The extended Higgs sector is presented in the next section and studied in more detail in Appendix A. For a set of quartic couplings for S and $H_{1,2}$ that are relevant for electroweak symmetry and $U(1)'$ breaking, we have collected unitarity bounds in Appendix B, which are used to constrain the parameter space of the Higgs sector in Sect. 4.

The Yukawa Lagrangian for quarks and leptons is given by

$$-\mathcal{L}_Y = \bar{q}_i (y^u_{ij} \tilde{H}_1 + h^u_{ij} \tilde{H}_2) u_j + \bar{q}_i (y^d_{ij} H_1 + h^d_{ij} H_2) d_j + y^\ell_{ij} \bar{\ell}_i H_1 e_j + y^\nu_{ij} \bar{\ell}_i \tilde{H}_1 \nu_{jR} + \overline{(\nu_{iR})^c} (M_{ij} + \Phi_a z^{(a)}_{ij}) \nu_{jR} + \text{h.c.} \tag{2.5}$$

with $\tilde{H}_{1,2} \equiv i\sigma_2 H^*_{1,2}$. After electroweak symmetry and $U(1)'$ are broken by the VEVs of scalar fields, $\langle H_{1,2} \rangle = v_{1,2}/\sqrt{2}$ with $v_1^2 + v_2^2 = v^2 = (246\,\text{GeV})^2$, $\langle S \rangle = v_s/\sqrt{2}$ and $\langle \Phi_a \rangle = \omega_a/\sqrt{2}$, the quark and lepton mass terms are given as

$$\mathcal{L}_Y = -\bar{u} M_u u - \bar{d} M_d d - \bar{\ell} M_\ell \ell - \bar{\ell} M_D \nu_R - \overline{(\nu_R)^c} M_R \nu_R + \text{h.c.} \tag{2.6}$$

with the following flavor structure:

$$M_u = \begin{pmatrix} y^u_{11}\langle \tilde{H}_1 \rangle & y^u_{12}\langle \tilde{H}_1 \rangle & 0 \\ y^u_{21}\langle \tilde{H}_1 \rangle & y^u_{22}\langle \tilde{H}_1 \rangle & 0 \\ h^u_{31}\langle \tilde{H}_2 \rangle & h^u_{32}\langle \tilde{H}_2 \rangle & y^u_{33}\langle \tilde{H}_1 \rangle \end{pmatrix}, \tag{2.7}$$

$$M_d = \begin{pmatrix} y^d_{11}\langle H_1 \rangle & y^d_{12}\langle H_1 \rangle & h^d_{13}\langle H_2 \rangle \\ y^d_{21}\langle H_1 \rangle & y^d_{22}\langle H_1 \rangle & h^d_{23}\langle H_2 \rangle \\ 0 & 0 & y^d_{33}\langle H_1 \rangle \end{pmatrix}, \tag{2.8}$$

$$M_\ell = \begin{pmatrix} y^\ell_{11}\langle H_1 \rangle & 0 & 0 \\ 0 & y^\ell_{22}\langle H_1 \rangle & 0 \\ 0 & 0 & y^\ell_{33}\langle H_1 \rangle \end{pmatrix}, \tag{2.9}$$

$$M_D = \begin{pmatrix} y^\nu_{11}\langle \tilde{H}_1 \rangle & 0 & 0 \\ 0 & y^\nu_{22}\langle \tilde{H}_1 \rangle & 0 \\ 0 & 0 & y^\nu_{33}\langle \tilde{H}_1 \rangle \end{pmatrix}, \tag{2.10}$$

$$M_R = \begin{pmatrix} M_{11} & z^{(1)}_{12}\langle \Phi_1 \rangle & z^{(2)}_{13}\langle \Phi_2 \rangle \\ z^{(1)}_{21}\langle \Phi_1 \rangle & 0 & z^{(3)}_{23}\langle \Phi_3 \rangle \\ z^{(2)}_{31}\langle \Phi_2 \rangle & z^{(3)}_{32}\langle \Phi_3 \rangle & 0 \end{pmatrix}. \tag{2.11}$$

Since the mass matrix for charged leptons is already diagonal, the lepton mixings come from the mass matrix of RH neutrinos. There are four other categories of neutrino mixing matrices [14,15], that are compatible with neutrino data. In all the cases, we need at least three complex scalar fields with different $U(1)'$ charges, similarly to the case given in (2.11). The quark Yukawa couplings to Higgs bosons are summarized in Appendix C.

We find the Z-like (Z_1) and Z'-like (Z_2) masses as

$$m^2_{Z_{1,2}} = \frac{1}{2}\left(m_Z^2 + m_{22}^2 \mp \sqrt{(m_Z^2 - m_{22}^2)^2 + 4m_{12}^4} \right), \tag{2.12}$$

where $m_Z^2 \equiv (g^2 + g_Y^2)v^2/4$, and

$$m_{22}^2 \equiv m_Z^2 s_W^2 t_\xi^2 + m_{Z'}^2/c_\xi^2 - c_W^{-1} e g_{Z'} Q'_{H_2} v_w^2 t_\xi / c_\xi,$$
$$m_{12}^2 \equiv m_Z^2 s_W t_\xi - \frac{1}{2} c_W^{-1} s_W^{-1} e g_{Z'} Q'_{H_2} v_2^2 / c_\xi \tag{2.13}$$

with

$$m^2_{Z'} = g^2_{Z'} \left(\frac{1}{9} x^2 v_s^2 + y^2 \omega_1^2 + (x+y)^2 \omega_2^2 + x^2 \omega_3^2 \right). \tag{2.14}$$

Here $s_\varphi \equiv \sin\varphi$, $c_\varphi \equiv \cos\varphi$, and $t_\varphi \equiv \tan\varphi$. The modified Z boson mass can receive constraints from electroweak precision data, which is studied in Sect. 4. We note that for a small mass mixing, the Z'-like mass is approximately given by $m^2_{Z_2} \approx m^2_{Z'}$ and we can treat $m_{Z'}$ and $g_{Z'}$ to be independent parameters due to the presence of nonzero ω_i's. The $U(1)'$ interactions are collected in Appendix D.

3 Higgs spectrum and Yukawa couplings

We here specify the Higgs spectrum of our model and identify the quark and lepton Yukawa couplings of neutral and charged Higgs bosons for studies in next sections. The expressions are based on results in Appendices A and C .

3.1 The Higgs spectrum

The Higgs sector of our model has two Higgs doublets, which are expressed in components as

$$H_j = \begin{pmatrix} \phi_j^+ \\ (v_j + \rho_j + i\eta_j)/\sqrt{2} \end{pmatrix} \quad (j = 1, 2), \tag{3.1}$$

and the complex singlet scalar decomposed into $S = (v_s + S_R + iS_I)/\sqrt{2}$.

In the limit of negligible mixing with the CP-even singlet scalar, the mass eigenstates of CP-even neutral Higgs scalars, h and H, are given by

$$h = -\sin\alpha\,\rho_1 + \cos\alpha\,\rho_2,$$
$$H = \cos\alpha\,\rho_1 + \sin\alpha\,\rho_2. \tag{3.2}$$

The general case where the CP-even part of the singlet scalar S mixes with the Higgs counterpart is considered in Appendix A. The mass eigenvalues of CP-even neutral Higgs scalars are denoted as $m_{h_{1,2,3}}$ with $m_{h_1} < m_{h_2} < m_{h_3}$, alternatively, $m_h \equiv m_{h_1}$, $m_H \equiv m_{h_2}$ and $m_s \equiv m_{h_3}$, and there are three mixing angles, $\alpha_{1,2,3}$: $\alpha_1 = \alpha$ in the limit of a decoupled CP-even singlet scalar, while α_2 and α_3 are mixing angles between $\rho_{1,2}$ and S_R, respectively. For $2\kappa_1 v_1 v_s \approx \mu v_2/\sqrt{2}$ and $2\kappa_2 v_2 v_s \approx \mu v_1/\sqrt{2}$, the mixing between $\rho_{1,2}$ and S_R can be neglected. For a later discussion, we focus mainly on this case.

The CP-odd parts of the singlet scalars, S and Φ_a, can mix with the Higgs counterpart due to a nonzero $U(1)'$ charge of the second Higgs H_2, but for a small x and small VEV of H_2, the mixing effect is negligible. In this case, the neutral Goldstone boson G^0 and the CP-odd Higgs scalar A^0 are turned out to be

$$G^0 = \cos\beta\,\eta_1 + \sin\beta\,\eta_2,$$
$$A^0 = \sin\beta\,\eta_1 - \cos\beta\,\eta_2 \tag{3.3}$$

with $\tan\beta \equiv v_2/v_1$. The massless combination of η_1 and η_2 is eaten by the Z boson, while a linear combination of S_I and other pseudoscalars of Φ_a is eaten by the Z' boson if the Z' mass is determined dominantly by the VEV of S. The other combination of the CP-odd scalars from two Higgs doublets has the mass of

$$m_A^2 = \frac{\mu\sin\beta\cos\beta}{\sqrt{2}v_s}\left(v^2 + \frac{v_s^2}{\sin^2\beta\cos^2\beta}\right). \tag{3.4}$$

On the other hand, the charged Goldstone bosons G^+ and charged Higgs scalar H^+ identified as

$$G^+ = \cos\beta\,\phi_1^+ + \sin\beta\,\phi_2^+,$$
$$H^+ = \sin\beta\,\phi_1^+ - \cos\beta\,\phi_2^+ \tag{3.5}$$

with nonzero mass eigenvalue given by

$$m_{H^+}^2 = m_A^2 - \left(\frac{\mu\sin\beta\cos\beta}{\sqrt{2}v_s} + \lambda_4\right)v^2. \tag{3.6}$$

We remark that in the limit of $\mu v_s \gg v^2$, the heavy scalars in the Higgs doublets become almost degenerate as $m_A^2 \approx m_H^2 \approx m_{H^+}^2 \approx \mu v_s/(\sqrt{2}\sin\beta\cos\beta)$ and $m_s^2 \approx 2\lambda_S v_s^2$ from Eqs. (3.4), (3.6) and (A.5). In this limit, the mixing angles between the SM-like Higgs and extra scalars can be negligibly small and the resulting Higgs spectrum is consistent with Higgs data and electroweak precision tests (EWPT) as will be discussed in Subsec 4.2. But, as μv_s is constrained by perturbativity and unitarity bounds on the quartic couplings with Eqs. (A.7) or (A.9), as will be discussed in Sect. 4, the extra scalars in our model remain non-decoupled. Since it is sufficient to take almost degenerate masses for two of m_A, m_H, and m_{H^+} for EWPT, we henceforth consider more general scalar masses but with small mixings between the SM-like Higgs and the extra neutral scalars.

3.2 Quark mass matrices

We now consider the quark mass matrices and their diagonalization. After two Higgs doublets develop VEVs, we obtain the quark mass matrices from Eqs. (2.7) and (2.8) as

$$(M_u)_{ij} = \frac{1}{\sqrt{2}}v\cos\beta\begin{pmatrix} y_{11}^u & y_{12}^u & 0 \\ y_{21}^u & y_{22}^u & 0 \\ 0 & 0 & y_{33}^u \end{pmatrix} + \frac{1}{\sqrt{2}}v\sin\beta\begin{pmatrix} 0 & 0 & 0 \\ 0 & 0 & 0 \\ h_{31}^u & h_{32}^u & 0 \end{pmatrix}, \tag{3.7}$$

$$(M_d)_{ij} = \frac{1}{\sqrt{2}}v\cos\beta\begin{pmatrix} y_{11}^d & y_{12}^d & 0 \\ y_{21}^d & y_{22}^d & 0 \\ 0 & 0 & y_{33}^d \end{pmatrix} + \frac{1}{\sqrt{2}}v\sin\beta\begin{pmatrix} 0 & 0 & h_{13}^d \\ 0 & 0 & h_{23}^d \\ 0 & 0 & 0 \end{pmatrix}. \tag{3.8}$$

The quark mass matrices can be diagonalized by

$$U_L^\dagger M_u U_R = M_u^D = \begin{pmatrix} m_u & 0 & 0 \\ 0 & m_c & 0 \\ 0 & 0 & m_t \end{pmatrix},$$
$$D_L^\dagger M_d D_R = M_d^D = \begin{pmatrix} m_d & 0 & 0 \\ 0 & m_s & 0 \\ 0 & 0 & m_b \end{pmatrix}, \tag{3.9}$$

thus the CKM matrix is given as $V_{\rm CKM} = U_L^\dagger D_L$. We note that the Yukawa couplings of the second Higgs doublet are sources of flavor violation, which could be important in meson decays/mixings and collider searches for flavor-violating top decays and/or heavy Higgs bosons [16–19]. The detailed derivation of flavor-violating Higgs couplings is presented in the next section.

Since h^u_{31} and h^u_{32} correspond to rotations of right-handed up-type quarks, we can take $U_L = 1$, so $V_{\rm CKM} = D_L$. In this case, we have an approximate relation for the down-type quark mass matrix, $M_d \approx V_{\rm CKM} M^D_d$, up to $m_{d,s}/m_b$ corrections. Then the Yukawa couplings between the third and first two generations are given as follows.

$$h^d_{13} = \frac{\sqrt{2}m_b}{v\sin\beta}\, V_{ub}, \quad h^d_{23} = \frac{\sqrt{2}m_b}{v\sin\beta}\, V_{cb}. \tag{3.10}$$

For $V_{ub} \simeq 0.004 \ll V_{cb} \simeq 0.04$, we have $h^d_{13} \ll h^d_{23}$. The down-type Yukawa couplings are determined as

$$\begin{aligned} &y^d_{11} = \frac{\sqrt{2}m_d}{v\cos\beta}\, V_{ud}, \quad y^d_{12} = \frac{\sqrt{2}m_s}{v\cos\beta}\, V_{us}, \\ &y^d_{21} = \frac{\sqrt{2}m_d}{v\cos\beta}\, V_{cd}, \quad y^d_{22} = \frac{\sqrt{2}m_s}{v\cos\beta}\, V_{cs}, \quad y^d_{33} = \frac{\sqrt{2}m_b}{v\cos\beta}\, V_{tb}. \end{aligned} \tag{3.11}$$

On the other hand, taking $U_L = 1$ as above, we find another approximate relation for the up-type quark mass matrix: $M_u = M^D_u U^\dagger_R$. Then the rotation mass matrix for right-handed down-type quarks becomes $U^\dagger_R = (M^D_u)^{-1} M_u$, which is given as

$$U^\dagger_R = \frac{1}{\sqrt{2}} \begin{pmatrix} \frac{v}{m_u}\cos\beta\, y^u_{11} & \frac{v}{m_u}\cos\beta\, y^u_{12} & 0 \\ \frac{v}{m_c}\cos\beta\, y^u_{21} & \frac{v}{m_c}\cos\beta\, y^u_{22} & 0 \\ \frac{v}{m_t}\sin\beta\, h^u_{31} & \frac{v}{m_t}\sin\beta\, h^u_{32} & \frac{v}{m_t}\cos\beta\, y^u_{33} \end{pmatrix}. \tag{3.12}$$

From the unitarity condition of U_R we further find the following constraints on the up-type quark Yukawa couplings:

$$|y^u_{11}|^2 + |y^u_{12}|^2 = \frac{2m_u^2}{v^2\cos^2\beta}, \tag{3.13}$$

$$|y^u_{21}|^2 + |y^u_{22}|^2 = \frac{2m_c^2}{v^2\cos^2\beta}, \tag{3.14}$$

$$|y^u_{33}|^2 + \tan^2\beta(|h^u_{31}|^2 + |h^u_{32}|^2) = \frac{2m_t^2}{v^2\cos^2\beta}, \tag{3.15}$$

$$y^u_{11}(y^u_{21})^* + y^u_{12}(y^u_{22})^* = 0, \tag{3.16}$$

$$y^u_{21}(h^u_{31})^* + y^u_{22}(h^u_{32})^* = 0, \tag{3.17}$$

$$y^u_{11}(h^u_{31})^* + y^u_{12}(h^u_{32})^* = 0. \tag{3.18}$$

3.3 Quark Yukawa couplings

Using the results in Appendix C, we get the Yukawa interactions for the SM-like Higgs boson h and heavy neutral Higgs bosons H, A as

$$\begin{aligned} -\mathcal{L}^{h/H/A}_Y = &\frac{\cos(\alpha-\beta)}{\sqrt{2}\cos\beta}\bar{b}_R(\tilde{h}^{d*}_{13}d_L + \tilde{h}^{d*}_{23}s_L)h \\ &+ \frac{\lambda^h_b}{\sqrt{2}}\bar{b}_R b_L h + \frac{\lambda^h_t}{\sqrt{2}}\bar{t}_R t_L h \\ &+ \frac{\sin(\alpha-\beta)}{\sqrt{2}\cos\beta}\bar{b}_R(\tilde{h}^{d*}_{13}d_L + \tilde{h}^{d*}_{23}s_L)H \\ &+ \frac{\lambda^H_b}{\sqrt{2}}\bar{b}_R b_L H + \frac{\lambda^H_t}{\sqrt{2}}\bar{t}_R t_L H \\ &- \frac{i}{\sqrt{2}\cos\beta}\bar{b}_R(\tilde{h}^{d*}_{13}d_L + \tilde{h}^{d*}_{23}s_L)A \\ &+ \frac{i\lambda^A_b}{\sqrt{2}}\bar{b}_R b_L A - \frac{i\lambda^A_t}{\sqrt{2}}\bar{t}_R t_L A + \text{h.c.} \end{aligned} \tag{3.19}$$

where

$$\lambda^h_b = -\frac{\sqrt{2}m_b\sin\alpha}{v\cos\beta} + \frac{\tilde{h}^d_{33}\cos(\alpha-\beta)}{\cos\beta}, \tag{3.20}$$

$$\lambda^h_t = -\frac{\sqrt{2}m_t\sin\alpha}{v\cos\beta} + \frac{\tilde{h}^u_{33}\cos(\alpha-\beta)}{\cos\beta}, \tag{3.21}$$

$$\lambda^H_b = \frac{\sqrt{2}m_b\cos\alpha}{v\cos\beta} + \frac{\tilde{h}^d_{33}\sin(\alpha-\beta)}{\cos\beta}, \tag{3.22}$$

$$\lambda^H_t = \frac{\sqrt{2}m_t\cos\alpha}{v\cos\beta} + \frac{\tilde{h}^u_{33}\sin(\alpha-\beta)}{\cos\beta}, \tag{3.23}$$

$$\lambda^A_b = \frac{\sqrt{2}m_b\tan\beta}{v} - \frac{\tilde{h}^d_{33}}{\cos\beta}, \tag{3.24}$$

$$\lambda^A_t = \frac{\sqrt{2}m_t\tan\beta}{v} - \frac{\tilde{h}^u_{33}}{\cos\beta}. \tag{3.25}$$

We note that $\tilde{h}^d \equiv D^\dagger_L h^d D_R$ and $\tilde{h}^u \equiv U^\dagger_L h^u U_R$. Thus, by taking $U_L = 1$ we get $\tilde{h}^u = h^u U_R$ and $\tilde{h}^d = V^\dagger_{\rm CKM} h^d$. In this case, as compared to two-Higgs-doublet model type I, extra Yukawa couplings are given by

$$\tilde{h}^u_{33} = \frac{\sqrt{2}m_t}{v\sin\beta}\left(1 - \frac{v^2\cos^2\beta}{2m_t^2}|y^u_{33}|^2\right), \tag{3.26}$$

$$\tilde{h}^d_{13} = 1.80\times10^{-2}\left(\frac{m_b}{v\sin\beta}\right), \tag{3.27}$$

$$\tilde{h}^d_{23} = 5.77\times10^{-2}\left(\frac{m_b}{v\sin\beta}\right), \tag{3.28}$$

$$\tilde{h}^d_{33} = 2.41\times10^{-3}\left(\frac{m_b}{v\sin\beta}\right). \tag{3.29}$$

We find that the flavor-violating couplings for light up-type quarks vanish, while the top quark Yukawa can have a sizable modification due to nonzero $\tilde{h}^u_{33}$. On the other hand, the flavor-violating couplings for down-type quarks can be large if $\tan\beta$ is small, even though the couplings have the suppression factors of CKM mixing and smallness of bottom quark mass. The couplings can be constrained by bounds

from B-meson mixings and decays as is discussed in the next section. We note that the flavor-violating interactions of the SM-like Higgs boson are turned off in the alignment limit where $\alpha = \beta - \pi/2$.

The Yukawa terms of the charged Higgs boson are given as

$$\begin{aligned} -\mathcal{L}_Y^{H^-} &= \bar{b}(\lambda_{t_L}^{H^-} P_L + \lambda_{t_R}^{H^-} P_R) t H^- \\ &\quad + \bar{b}(\lambda_{c_L}^{H^-} P_L + \lambda_{c_R}^{H^-} P_R) c H^- \\ &\quad + \lambda_{u_L}^{H^-} \bar{b} P_L u H^- + \text{h.c.}, \end{aligned} \tag{3.30}$$

where

$$\lambda_{t_L}^{H^-} = \frac{\sqrt{2} m_b \tan\beta}{v} V_{tb}^* - \frac{(V_{\text{CKM}} \tilde{h}^d)_{33}^*}{\cos\beta}, \tag{3.31}$$

$$\lambda_{t_R}^{H^-} = -\left(\frac{\sqrt{2} m_t \tan\beta}{v} - \frac{\tilde{h}_{33}^u}{\cos\beta} \right) V_{tb}^*, \tag{3.32}$$

$$\lambda_{c_L}^{H^-} = \frac{\sqrt{2} m_b \tan\beta}{v} V_{cb}^* - \frac{(V_{\text{CKM}} \tilde{h}^d)_{23}^*}{\cos\beta}, \tag{3.33}$$

$$\lambda_{c_R}^{H^-} = -\frac{\sqrt{2} m_c \tan\beta}{v} V_{cb}^*, \tag{3.34}$$

$$\lambda_{u_L}^{H^-} = \frac{\sqrt{2} m_b \tan\beta}{v} V_{ub}^* - \frac{(V_{\text{CKM}} \tilde{h}^d)_{13}^*}{\cos\beta} \tag{3.35}$$

with

$$V_{\text{CKM}} \tilde{h}^d = \begin{pmatrix} 0 & 0 & V_{ud} \tilde{h}_{13}^d + V_{us} \tilde{h}_{23}^d + V_{ub} \tilde{h}_{33}^d \\ 0 & 0 & V_{cd} \tilde{h}_{13}^d + V_{cs} \tilde{h}_{23}^d + V_{cb} \tilde{h}_{33}^d \\ 0 & 0 & V_{td} \tilde{h}_{13}^d + V_{ts} \tilde{h}_{23}^d + V_{tb} \tilde{h}_{33}^d \end{pmatrix}. \tag{3.36}$$

If $y_{33}^u = y_t^{\text{SM}} = \sqrt{2} m_t / v$, the Higgs coupling to top quark becomes

$$\lambda_t^H = y_t^{\text{SM}} \cos(\alpha - \beta), \tag{3.37}$$

and $\lambda_t^A = \lambda_{t_R}^{H^-} = 0$.

3.4 Lepton Yukawa couplings

As seen in (2.9), the mass matrix for charged leptons e_j is already diagonal due to the $U(1)'$ symmetry. Thus, the lepton Yukawa couplings are in a flavor-diagonal form given by

$$\begin{aligned} -\mathcal{L}_Y^{\ell} &= -\frac{m_{e_j} \sin\alpha}{v \cos\beta} \bar{e}_j e_j h + \frac{m_{e_j} \cos\alpha}{v \cos\beta} \bar{e}_j e_j H \\ &\quad + \frac{i m_{e_j} \tan\beta}{v} \bar{e}_j \gamma^5 e_j A^0 \\ &\quad + \frac{\sqrt{2} m_{e_j} \tan\beta}{v} \left(\bar{\nu}_j P_R e_j H^+ + \text{h.c.} \right) \end{aligned} \tag{3.38}$$

4 Constraints on the Higgs sector

In this section we consider various phenomenological constraints on the model coming from B-meson mixings and decays as well as Higgs and electroweak precision data on top of unitarity and stability bounds on the Higgs sector. We also show how to explain the deficits in R_K and R_{K^*} in the B-meson decays at LHCb in our model, and discuss the predictions for R_D and R_{D^*} through the charged Higgs exchange.

4.1 Unitarity and stability bounds

Before considering the phenomenological constraints, we consider unitarity and stability bounds for the Higgs sector. As derived in Appendix B, the conditions for perturbativity and unitarity are

$$\begin{aligned} |\lambda_{1,2,3,S}| \le 4\pi, &\quad |\kappa_{1,2}| \le 4\pi, \\ |\lambda_3 \pm \lambda_4| \le 4\pi, &\quad |\lambda_3 + 2\lambda_4| \le 4\pi, \\ \sqrt{\lambda_3(\lambda_3 + 2\lambda_4)} &\le 4\pi, \\ |\lambda_1 + \lambda_2 \pm \sqrt{(\lambda_1 - \lambda_2)^2 + 4\lambda_4^2}| &\le 8\pi \\ a_{1,2,3} &\le 8\pi, \end{aligned} \tag{4.1}$$

where $a_{1,2,3}$ are the solutions to Eq. (B.7). The vacuum stability conditions of the scalar potential can be obtained by considering the potential to be bounded from below along the directions of large Higgs doublet and singlet scalar fields. Following Refs. [20–22], we obtain the stability conditions as follows:

$$\begin{aligned} &\lambda_{1,2,S} > 0 \\ &\sqrt{\lambda_1 \lambda_2} + \lambda_3 + \lambda_4 > 0, \\ &\sqrt{\lambda_1 \lambda_2} + \lambda_3 > 0, \\ &\sqrt{\lambda_1 \lambda_S} + \kappa_1 > 0, \\ &\sqrt{\lambda_2 \lambda_S} + \kappa_2 > 0, \\ &\sqrt{(\kappa_1^2 - \lambda_1 \lambda_S)(\kappa_2^2 - \lambda_2 \lambda_S)} + \lambda_3 \lambda_S > \kappa_1 \kappa_2, \\ &\sqrt{(\kappa_1^2 - \lambda_1 \lambda_S)(\kappa_2^2 - \lambda_2 \lambda_S)} + (\lambda_3 + \lambda_4) \lambda_S > \kappa_1 \kappa_2. \end{aligned} \tag{4.2}$$

The stability conditions along the other scalar fields Φ_a can be obtained in the similar way, but they are not relevant for our study because Φ_a's do not couple directly to Higgs doublets as long as the extra quartic couplings for Φ_a are positive and large enough.

The unitarity and stability bounds are depicted in Figs. 1 and 2 for the parameter space in terms of m_{h_2} and $\tan\beta$, or v_s and μ, with assuming the alignment limit, $\cos(\alpha - \beta) = 0.05$, and zero mixing between heavy CP-even scalars. In each

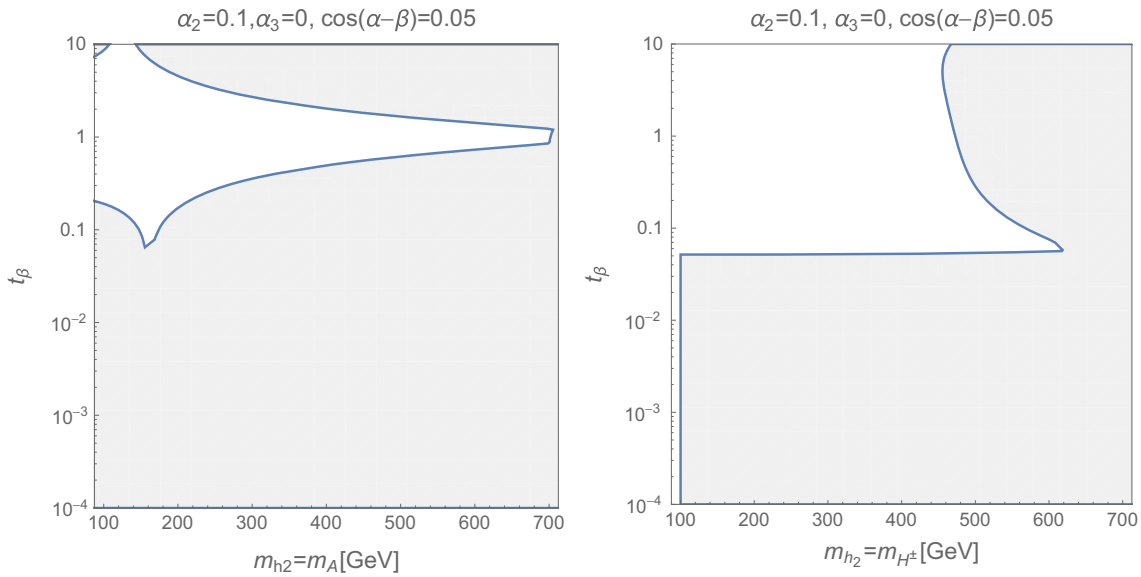

Fig. 1 Parameter space in terms of m_{h_2} and $\tan\beta$. The gray regions are excluded by unitarity and stability bounds. $v_s = 2m_{h_3} = 1$ TeV and $\cos(\alpha-\beta) = 0.05$ with $m_{h_2} = m_A$ and $m_{H^\pm} = 500$ GeV in the left, and $m_{h_2} = m_{H^\pm}$ and $m_A = 140$ GeV in the right panel. The mixing between heavy CP-even scalars is taken to be zero

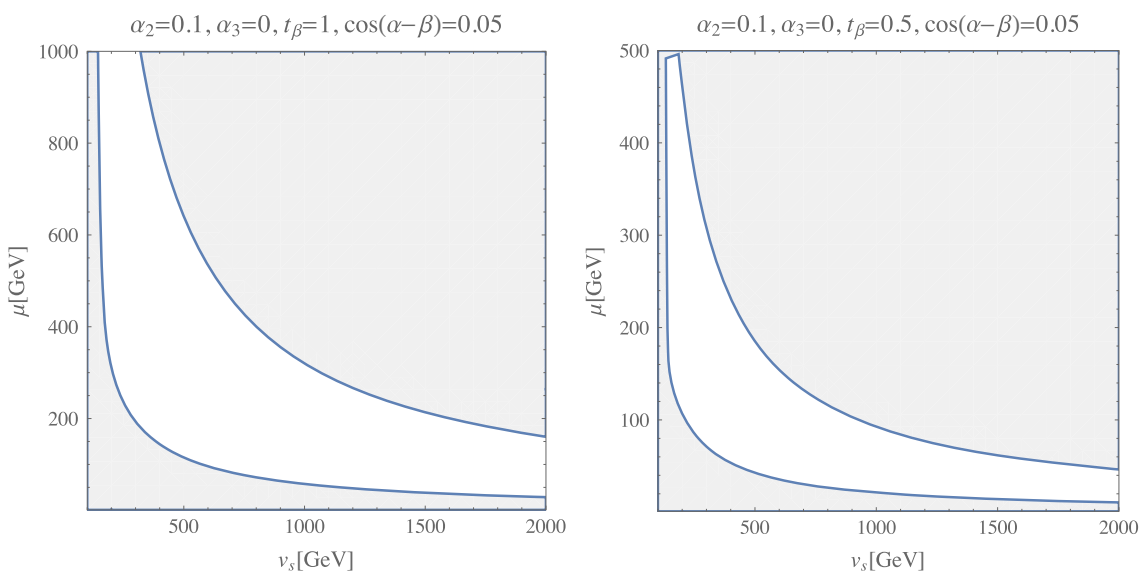

Fig. 2 Parameter space in terms of v_s and μ for $m_{h_3} = m_{H^\pm} = m_{h_2} = 0.5$ TeV and $\cos(\alpha-\beta) = 0.05$. The gray regions are excluded by unitarity and stability bounds. $\tan\beta = 1$ (0.5) in the left (right) panel. The mixing between heavy CP-even scalars is taken to be zero

figure, the gray region corresponds to the parameter space excluded by the unitarity and stability conditions. In Fig. 1, we have taken the different choices of Higgs masses: $m_{h_2} = m_A$ and $m_{H^\pm} = 500$ GeV in the left, while $m_{h_2} = m_{H^\pm}$ and $m_A = 140$ GeV in the right panel. On the other hand, the parameter space in terms of v_s and μ has been shown in Fig. 2, with setting $m_{h_3} = m_{H^\pm} = m_{h_2} = 0.5$ TeV, but taking different values of $\tan\beta$. We note that the unitarity and stability bounds are sensitive to the choice of $\tan\beta$, while insensitive to the mixing angle of heavy CP-even scalars, in constraining the mass parameters. The allowed parameter space for mass parameters becomes narrower as $\tan\beta$ is smaller.

4.2 Higgs and electroweak precision data

Provided that the Higgs mixings with the singlet scalar are small, the mixing angle α between CP-even Higgs scalars

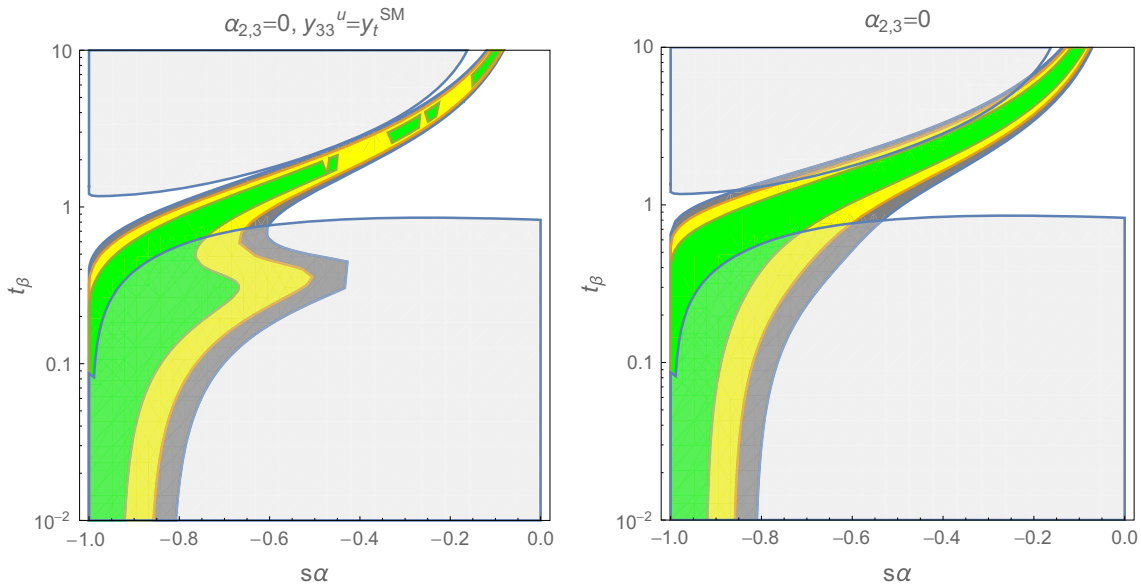

Fig. 3 Parameter space for $\sin\alpha$ and $\tan\beta$ allowed by Higgs data within 1σ (green), 2σ (yellow), and 3σ (dark gray). The gray regions corresponds to the unitarity and stability bounds. $y^u_{33} = y_t^{\rm SM}$ in the left and $y^u_{33} = y_t^{\rm SM}/\cos\beta$ in the right panel. $m_{h_2} = m_{H^\pm} = 450$ GeV, $m_A = 140$ GeV and $v_s = 1$ TeV has been taken in all panels

are constrained by Higgs precision data [23–32]. The parameter space for $\sin\alpha$ and $\tan\beta$ allowed by the Higgs data is shown in Fig. 3. We take the (33) component of the up-type Higgs Yukawa coupling to be $y^u_{33} = y_t^{\rm SM}$ in the left, and $y^u_{33} = y^{\rm SM}/\cos\beta$ in the right panel. For illustration, we have also imposed unitarity and stability bounds discussed in the previous subsection for $m_{h_2} = m_{H^\pm} = 450$ GeV, $m_A = 140$ GeV and $v_s = 1$ TeV. As a result, we find a wide parameter space close to the line of the alignment, $\alpha = \beta - \pi/2$, that is consistent with both the Higgs data and unitarity/stability bounds for $\tan\beta \gtrsim 0.1$. Thus, henceforth, for the phenomenology of the extra Higgs scalars, we focus on the parameter space near the alignment limit, $\cos(\alpha-\beta) \sim 0$.

To see bounds from electroweak precision data, we obtain effective Lagrangian after integrating out W and Z bosons as follows [33,34]:

$$\mathcal{L}_{\rm eff} = -\frac{4G_F}{\sqrt{2}g^2\sec^2\theta_W}\Big(\sec^2\theta_W J^\mu_{W^+}J_{W^-,\mu} + \rho J^\mu_Z J_{Z,\mu} + 2aJ^\mu_Z J_{Z',\mu} + bJ^\mu_{Z'}J_{Z',\mu}\Big) + \cdots, \tag{4.3}$$

where $J^\mu_Z = J^\mu_3 - \sin^2\theta_* J^\mu_{\rm EM}$ with θ_* being the modified Weinberg angle. Here the non-oblique terms, a and b, are determined at tree level as

$$a = \frac{\rho\sin\zeta\sec\xi}{\cos\zeta + \sin\theta_W\tan\xi\sin\zeta}, \quad b = \frac{a^2}{\rho}. \tag{4.4}$$

From the Z-boson like mass given in Eq. (D.6) and the Z–Z' mixing angle in Eq. (D.7), we find the correction to the ρ parameter as

$$\Delta\rho = \frac{m_W^2}{m_{Z_1}^2\cos^2\theta_W}(\cos\zeta + \sin\theta_W\tan\xi\sin\zeta)^2 - 1 \simeq \frac{\sin^2\theta_W}{\cos^2\xi}\frac{m_Z^2}{m_{Z'}^2}\left[\left(2Q'_{H_2}\frac{g_{Z'}}{g_Y}\right)^2\sin^4\beta - \sin^2\xi\right], \tag{4.5}$$

where we assumed that $\tan 2\zeta \simeq 2m_{12}^2/m_{Z_2}^2 \ll 1$. Taking the limit of zero gauge kinetic mixing, i.e. $\sin\xi = 0$, we have

$$\Delta\rho = \frac{m_W^2}{m_Z^2\cos^2\theta_W} - 1 \simeq 10^{-4}\left(\frac{x}{0.05}\right)^2 g_{Z'}^2\sin^4\beta\left(\frac{400\,\text{GeV}}{m_{Z'}}\right)^2, \tag{4.6}$$

which is consistent with the result in Ref. [12]. Therefore, for $\tan\beta \simeq 1$, $g_{Z'} \simeq 1$, and $x \simeq 0.05$, Z' with the mass $m_{Z'} \gtrsim 400\,\text{GeV}$ is consistent with electroweak precision data. The mass splittings between extra Higgs scalars can also be constrained by the electroweak precision data, but it can be easily satisfied if we take $m_{h_2} = m_{H^\pm}$ or $m_{h_2} = m_A$, and a small mixing between CP-even scalars.

4.3 B-meson anomalies from Z'

Before considering constraints from B-meson mixings and decays, we show how to explain the B-meson anomalies in

our model and identify the relevant parameter space for that. This section is based on the detailed results on $U(1)'$ interactions presented in Appendix D and phenomenological findings in Ref. [12].

From the relevant Z' interactions for B-meson anomalies and the Z' mass term,

$$\mathcal{L}'_{Z'} = g_{Z'} Z'_\mu \left(\frac{1}{3} x\, V_{ts}^* V_{tb}\, \bar{s}\gamma^\mu P_L b + \text{h.c.} + y \bar{\mu}\gamma^\mu \mu \right) + \frac{1}{2} m_{Z'}^2 Z'^2_\mu, \tag{4.7}$$

we get the classical equation of motion for Z' as

$$Z'_\mu = -\frac{g_{Z'}}{m_{Z'}^2} \left(\frac{1}{3} x\, V_{ts}^* V_{tb}\, \bar{s}\gamma_\mu P_L b + \text{h.c.} + y \bar{\mu}\gamma_\mu \mu \right). \tag{4.8}$$

Then, by integrating out the Z' gauge boson, we obtain the effective four-fermion interaction for $\bar{b} \to \bar{s}\mu^+\mu^-$ as follows.

$$\mathcal{L}_{\text{eff},\bar{b}\to\bar{s}\mu^+\mu^-} = -\frac{x y g_{Z'}^2}{3 m_{Z'}^2} V_{ts}^* V_{tb} (\bar{s}\gamma^\mu P_L b)(\bar{\mu}\gamma_\mu \mu) + \text{h.c.} \tag{4.9}$$

Consequently, as compared to the effective Hamiltonian with the SM normalization,

$$\Delta\mathcal{H}_{\text{eff},\bar{b}\to\bar{s}\mu^+\mu^-} = -\frac{4G_F}{\sqrt{2}} V_{ts}^* V_{tb} \frac{\alpha_{\text{em}}}{4\pi} C_9^{\mu,\text{NP}} \mathcal{O}_9^\mu \tag{4.10}$$

with $\mathcal{O}_9^\mu \equiv (\bar{s}\gamma^\mu P_L b)(\bar{\mu}\gamma_\mu \mu)$ and α_{em} being the electromagnetic coupling, we obtain new physics contribution to the Wilson coefficient,

$$C_9^{\mu,\text{NP}} = -\frac{8 x y \pi^2 \alpha_{Z'}}{3\alpha_{\text{em}}} \left(\frac{v}{m_{Z'}} \right)^2 \tag{4.11}$$

with $\alpha_{Z'} \equiv g_{Z'}^2/(4\pi)$, and vanishing contributions to other operators, $C_{10}^{\mu,\text{NP}} = C_9^{\prime\mu,\text{NP}} = C_{10}^{\prime\mu,\text{NP}} = 0$. We note that $xy > 0$ is chosen for a negative sign of C_9^μ, being consistent with B-meson anomalies. Requiring the best-fit value, $C_9^{\mu,\text{NP}} = -1.10$ [35–41], (while taking $[-1.27, -0.92]$ and $[-1.43, -0.74]$ within 1σ and 2σ errors), to explain the B-meson anomalies yields

$$m_{Z'} = 1.2\ \text{TeV} \times \left(x y \frac{\alpha_{Z'}}{\alpha_{\text{em}}} \right)^{1/2}. \tag{4.12}$$

Therefore, $m_{Z'} \simeq 1\,\text{TeV}$ for $xy \simeq 1$ and $\alpha_{Z'} \simeq \alpha_{\text{em}}$. For values of xy less than unity or $\alpha_{Z'} \lesssim \alpha_{\text{em}}$, Z' can be even lighter.

Various phenomenological constraints on the Z' interactions coming from dimuon resonance searches, other meson decays and mixing, tau lepton decays and neutrino scattering have been studied in Ref. [12], leading to the conclusion that the region of $x g_{Z'} \lesssim 0.05$ for $y g_{Z'} \simeq 1$ and $m_{Z'} \lesssim 1$ TeV is consistent with the parameter space for which the B-meson anomalies can be explained.

4.4 Bounds from B-meson mixings and decays

We now consider the bounds from B-meson mixings and decays. After integrating out the heavy Higgs bosons, the effective Lagrangian for $B_{s(d)} \to \mu^+\mu^-$ from the flavor-violating Yukawa interactions in (3.19) is

$$\begin{aligned}\Delta\mathcal{L}_{\text{eff},B_{s(d)}\to\mu^+\mu^-} &= -\frac{\sqrt{2} m_\mu \sin(\alpha-\beta)\cos\alpha}{2 m_H^2 v \cos\beta} \\ &\times ((\tilde{h}_{23}^d)^* \bar{b}_R s_L + (\tilde{h}_{13}^d)^* \bar{b}_R d_L + \text{h.c.})(\bar{\mu}\mu) \\ &- \frac{\sqrt{2} m_\mu \tan\beta}{2 m_A^2 v \cos\beta} \\ &\times ((\tilde{h}_{23}^d)^* \bar{b}_R s_L + (\tilde{h}_{13}^d)^* \bar{b}_R d_L + \text{h.c.})(\bar{\mu}\gamma^5\mu).\end{aligned} \tag{4.13}$$

The extra contributions to the effective Hamiltonian for $B_s \to \mu^+\mu^-$ are thus

$$\begin{aligned}\Delta\mathcal{H}_{\text{eff},B_s\to\mu^+\mu^-} &= -\frac{G_F^2 m_W^2}{\pi} \\ &\times [C_S^{\text{BSM}} (\bar{b} P_L s)(\bar{\mu}\mu) + C_P^{\text{BSM}} (\bar{b} P_L s)(\bar{\mu}\gamma^5\mu)]\end{aligned} \tag{4.14}$$

with

$$\begin{aligned}C_S^{\text{BSM}} &= -\frac{\pi}{G_F^2 m_W^2} \frac{\sqrt{2} m_\mu \sin(\alpha-\beta)\cos\alpha}{2 m_H^2 v \cos^2\beta} \cdot (\tilde{h}_{23}^d)^*, \\ C_P^{\text{BSM}} &= -\frac{\pi}{G_F^2 m_W^2} \frac{\sqrt{2} m_\mu \tan\beta}{2 m_A^2 v \cos\beta} \cdot (\tilde{h}_{23}^d)^*.\end{aligned} \tag{4.15}$$

In the alignment limit with $\alpha = \beta - \pi/2$ and $m_A \simeq m_H$, the Wilson coefficients become identical and suppressed for a small $\tan\beta$. The effective Hamiltonian in the above leads to the corrections of the branching ratio for $B_s \to \mu^+\mu^-$ as follows [42]:

$$\begin{aligned}\mathcal{B}(B_s \to \mu^+\mu^-) = \frac{G_F^4 m_W^4}{8\pi^5} \left(1 - \frac{4m_\mu^2}{m_{B_s}^2}\right)^{1/2} m_{B_s} f_{B_s}^2 m_\mu^2 \tau_{B_s} \\ \times \left[\left| \frac{m_{B_s}^2 (C_P - C'_P)}{2(m_b + m_s) m_\mu} - (C_A - C'_A) \right|^2 \right. \\ \left. + \left| \frac{m_{B_s}^2 (C_S - C'_S)}{2(m_b + m_s) m_\mu} \right|^2 \left(1 - \frac{4m_\mu^2}{m_{B_s}^2}\right) \right],\end{aligned} \tag{4.16}$$

where m_{B_s}, f_{B_s}, and τ_{B_s} are mass, decay constant, and lifetime of B_s-meson, respectively. $C_A^{(\prime)}, C_S^{(\prime)}, C_P^{(\prime)}$ are Wilson coefficients of the effective operators, $\mathcal{O}_A^{(\prime)} = [\bar{b}\gamma_\mu P_{L(R)}s][\bar{\mu}\gamma^\mu\gamma^5\mu]$, $\mathcal{O}_S^{(\prime)} = [\bar{b}P_{L(R)}s][\bar{\mu}\mu]$ and $\mathcal{O}_P^{(\prime)} = [\bar{b}P_{L(R)}s][\bar{\mu}\gamma^\mu\gamma^5\mu]$, respectively. We note that there is no contribution from Z' interactions to $B_s \to \mu^+\mu^-$ since the muon couplings to Z' are vector-like. On the other hand, in the alignment limit the bounds obtained from $B_{s,d} \to \mu^+\mu^-$ in Ref. [42] can be translated to our case as

$$\left|\tilde{h}^d_{23}\right| < 3.4 \times 10^{-2} \left(\frac{\cos\beta}{\tan\beta}\right)\left(\frac{m_{H,A}}{500\,\text{GeV}}\right)^2,$$
$$\left|\tilde{h}^d_{13}\right| < 1.7 \times 10^{-2} \left(\frac{\cos\beta}{\tan\beta}\right)\left(\frac{m_{H,A}}{500\,\text{GeV}}\right)^2. \tag{4.17}$$

From Eqs. (3.27) and (3.28), we find that flavor constraints are satisfied as far as

$$\sin\beta < \sqrt{1 - 0.033\left(\frac{500\,\text{GeV}}{m_{H,A}}\right)^2}. \tag{4.18}$$

This leads to $\tan\beta < 5.4$ for $m_{H,A} = 500\,\text{GeV}$.

The flavor-violating Yukawa couplings of heavy Higgs bosons as well as Z' interactions [12] can modify the B_s–$\bar{B}_s$ mixing. The additional effective Hamiltonian relevant for the mixing is given by

$$\Delta\mathcal{H}_{\text{eff},B_s-\bar{B}_s} = C_2'(\bar{s}_\alpha P_R b_\alpha)(\bar{s}_\beta P_R b_\beta) + \frac{G_F^2 m_W^2}{16\pi^2}(V_{ts}^* V_{tb})^2 C_{VLL}^{\text{NP}} \times (\bar{s}_\alpha\gamma^\mu P_L b_\alpha)(\bar{s}_\beta\gamma_\mu P_L b_\beta), \tag{4.19}$$

with

$$C_2' = \frac{\tilde{h}^d_{23}}{4\cos^2\beta\, m_H^2} \times \left(\frac{m_H^2}{m_A^2} - \sin^2(\alpha-\beta) - \frac{m_H^2\cos^2(\alpha-\beta)}{m_h^2}\right), \tag{4.20}$$

$$C_{VLL}^{\text{NP}} = \frac{16\pi^2}{9}\frac{(xg_{Z'})^2 v^4}{m_{Z'}^2 m_W^2} = 0.27\left(\frac{xg_{Z'}}{0.05}\right)^2\left(\frac{300\,\text{GeV}}{m_{Z'}}\right)^2. \tag{4.21}$$

The mass difference in the B_s system becomes

$$\Delta M_{B_s} = \frac{2}{3} m_{B_s} f_{B_s}^2 B_{123}^s(\mu) \times \left[\frac{G_F^2 m_W^2}{16\pi^2}(V_{ts}^* V_{tb})^2\left(C_{VLL}^{\text{SM}} + C_{VLL}^{\text{NP}}\right) + |C_2'|\right], \tag{4.22}$$

where $B_{123}^s(\mu)$ is a combination of bag-parameters [43] and $C_{VLL}^{\text{SM}} \simeq 4.95$ [44]. The SM prediction and the experimental values of ΔM_s are given by $(\Delta M_{B_s})^{\text{SM}} = (17.4 \pm 2.6)\,\text{ps}^{-1}$ [44] and $(\Delta M_{B_s})^{\text{exp}} = (17.757 \pm 0.021)\,\text{ps}^{-1}$ [45], respectively. Then, taking into account the SM uncertainties, we obtain the bounds on ΔM_{B_s} as $16\,(13)\,\text{ps}^{-1} < \Delta M_{B_s} < 21\,(23)\,\text{ps}^{-1}$ or $(\Delta M_{B_s})^{\text{BSM}} < 3.0\,(5.6)\,\text{ps}^{-1}$ at 1σ (2σ) level for new physics. We also note that the most recent lattice calculations show considerably large values for the bag parameters, leading to $(\Delta M_{B_s})^{\text{SM}} = (20.01 \pm 1.25)\,\text{ps}^{-1}$ [46]. It needs an independent confirmation, but if it is true, the new physics contributions coming from the heavy Higgs bosons and Z' would be constrained more tightly.

Taking the SM prediction as $(\Delta M_{B_s})^{\text{SM}} = (17.4 \pm 2.6)\,\text{ps}^{-1}$ [44], from Eq. (4.22) with Eqs. (4.20) and (4.21), we get the bound on the flavor-violating Yukawa coupling in the alignment limit of heavy Higgs bosons as

$$\frac{|\tilde{h}^d_{23}|}{\cos\beta}\left|\frac{m_H^2}{m_A^2} - 1\right|^{1/2}\left(\frac{500\,\text{GeV}}{m_H}\right) < 4.6(6.4) \times 10^{-3} \times\sqrt{1 - 0.1(0.06)\left(\frac{xg_{Z'}}{0.05}\right)^2\left(\frac{300\,\text{GeV}}{m_{Z'}}\right)^2}. \tag{4.23}$$

Here, since we need to choose $xg_{Z'} \lesssim 0.05$ for $m_{Z'} \lesssim 1\,\text{TeV}$ to satisfy the B-meson anomalies and the LHC dimuon bounds at the same time as discussed in the previous section, we can safely ignore the contribution of Z' interactions to the B_s–$\bar{B}_s$ mixing on the right-hand side of Eq. (4.23). Furthermore, with the Z' contribution ignored, the B_d–$\bar{B}_d$ mixing leads to a similar bound [43]:

$$\left|\tilde{h}^d_{13}\right| < 0.91(1.3) \times 10^{-3}\cos\beta\left|\frac{m_H^2}{m_A^2} - 1\right|^{-1/2}\left(\frac{m_H}{500\,\text{GeV}}\right). \tag{4.24}$$

Comparing to the bounds from $B_s \to \mu^+\mu^-$ in (4.17), the B–$\bar{B}$ mixings could lead to tighter constraints on the flavor-violating Yukawa couplings for down-type quarks unless m_H and m_A are almost degenerate. The upper frames of Fig. 4 show that a wide range of heavy Higgs masses up to 600–700 GeV are allowed for $m_{h_2} = m_A$ and $\tan\beta = \mathcal{O}(1)$. On the other hand, for $\tan\beta = 0.5$, the neutral Higgs boson can be as heavy as 400 GeV, but the charged Higgs mass is constrained as $240\,\text{GeV} \lesssim m_{H^\pm} \lesssim 650\,\text{GeV}$. For illustration, the case with $m_{h_2} = m_{H^\pm}$ has also been shown in the lower frames of Fig. 4, where the narrower region is allowed as compared with the case with $m_{h_2} = m_A$.

Another important bound comes from the inclusive radiative decay, $B \to X_s\gamma$. The effective Hamiltonian relevant for the $b \to s\gamma$ transition is

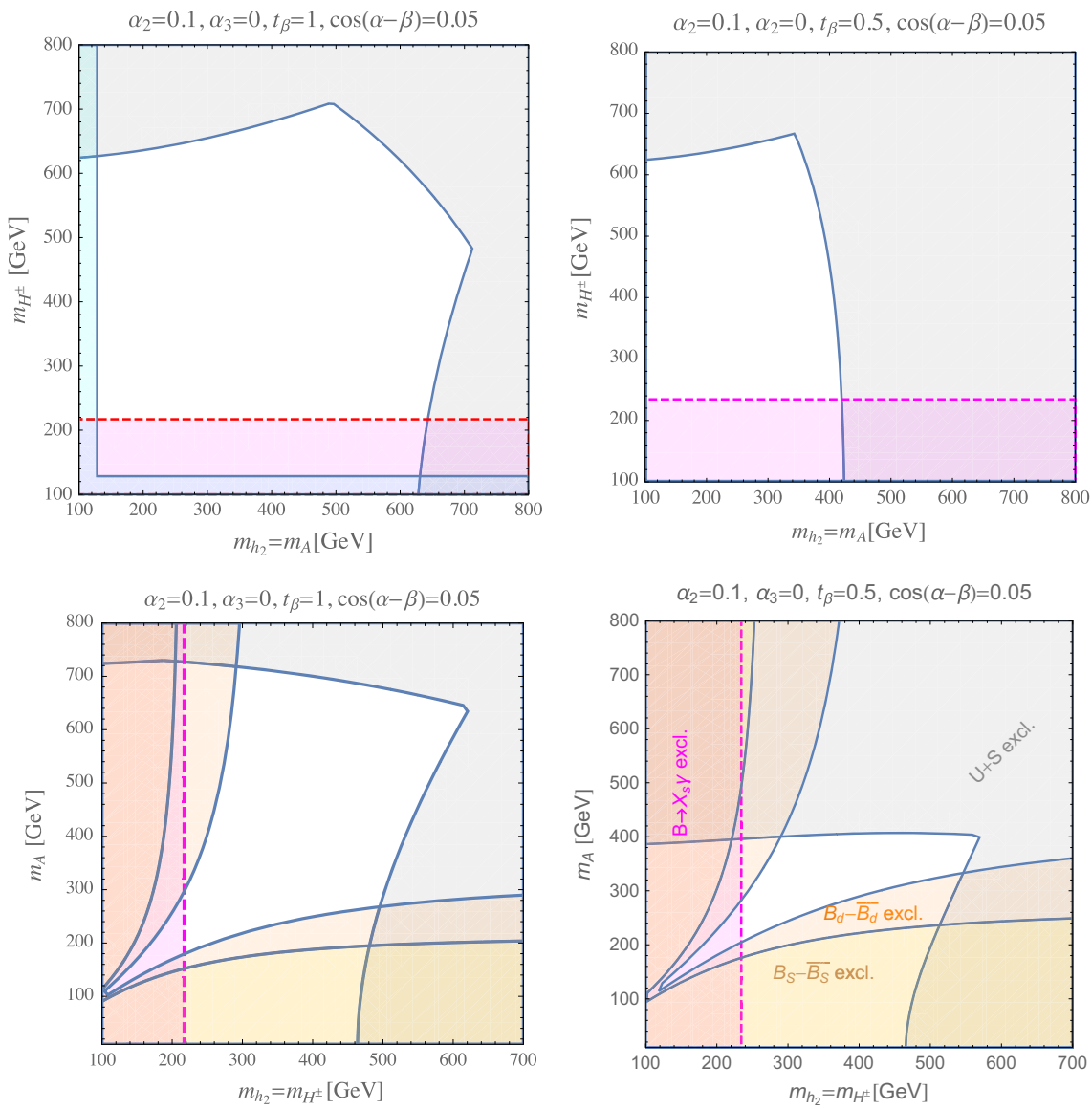

Fig. 4 Parameter space in terms of m_{h_2} and $m_{H^\pm}$ (upper frames), and m_A (lower frames). $\tan\beta = 1$ in the left and 0.5 in the right panels. We have chosen $v_s = 2m_{h_3} = 1$ TeV, $\cos(\alpha-\beta) = 0.05$, and $y^u_{33} = y_t^{\rm SM}$ in all frames. The mixing between heavy CP-even scalars is taken to be zero. The gray regions are excluded by unitarity and stability bounds. The magenta regions are excluded by $B \to X_s\gamma$, and cyan region is excluded by $B_s \to \mu^+\mu^-$. The yellow and orange regions are excluded by B_s and B_d mixings, respectively

$$\mathcal{H}_{\text{eff},b\to s\gamma} = -\frac{4G_F}{\sqrt{2}} V_{tb}V_{ts}^*(C_7\mathcal{O}_7 + C_8\mathcal{O}_8) \tag{4.25}$$

with

$$\mathcal{O}_7 = \frac{e}{16\pi^2} m_b\, \bar{s}\sigma^{\mu\nu} P_R b\, F_{\mu\nu},$$
$$\mathcal{O}_8 = \frac{g_s}{16\pi^2} m_b\, \bar{s}\sigma^{\mu\nu} P_R T^a b\, G^a_{\mu\nu}. \tag{4.26}$$

The charged Higgs contributions to the Wilson coefficients are given by [19,47]

$$C_7^{\rm BSM} = \frac{v^2}{2m_t^2}\frac{(\lambda_{t_R}^{H^-})^*\lambda_{t_R}^{H^-}}{V_{tb}V_{ts}^*} C_7^{(1)}(x_t) + \frac{v^2}{2m_t m_b}\frac{(\lambda_{t_L}^{H^-})^*\lambda_{t_R}^{H^-}}{V_{tb}V_{ts}^*} C_7^{(2)}(x_t),$$
$$C_8^{\rm BSM} = \frac{v^2}{2m_t^2}\frac{(\lambda_{t_R}^{H^-})^*\lambda_{t_R}^{H^-}}{V_{tb}V_{ts}^*} C_8^{(1)}(x_t) + \frac{v^2}{2m_t m_b}\frac{(\lambda_{t_L}^{H^-})^*\lambda_{t_R}^{H^-}}{V_{tb}V_{ts}^*} C_8^{(2)}(x_t) \tag{4.27}$$

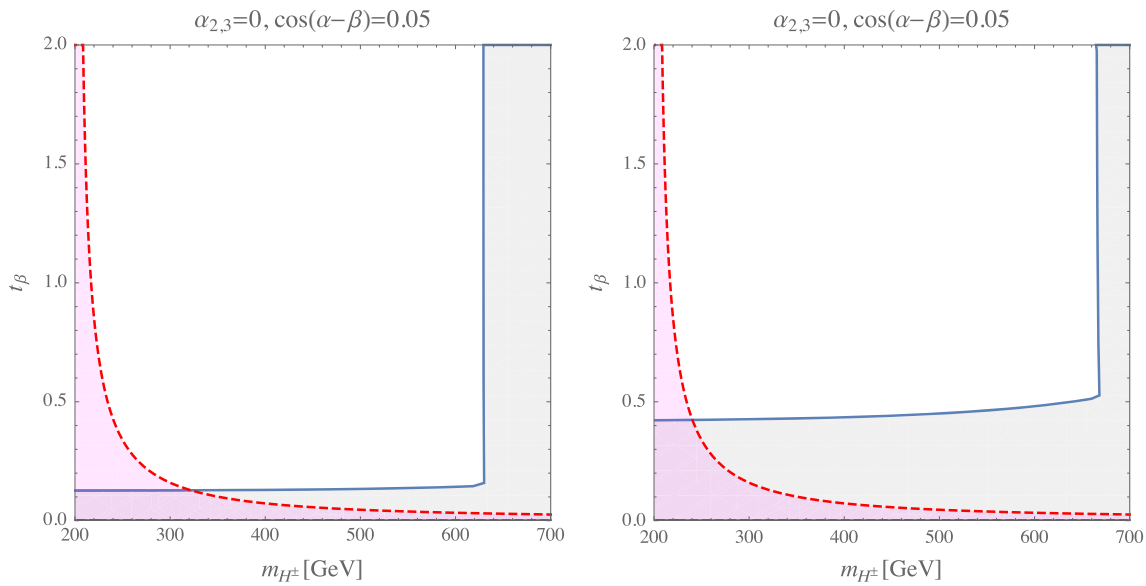

Fig. 5 Parameter space for $m_{H^\pm}$ and $\tan\beta$ excluded by $B \to X_s\gamma$ within 2σ (red) and unitarity bounds (gray) with $y^u_{33} = y_t^{\rm SM}$ for $m_A = m_{h_2} =$ 160 GeV (left panel) and $m_A = m_{h_2} = 350$ GeV (right panel)

with $x_t \equiv (m_t/m_{H^\pm})^2$, and

$$C_7^{(1)}(x) = \frac{x}{72}\left\{\frac{-8x^3+3x^2+12x-7+(18x^2-12)\ln x}{(x-1)^4}\right\},$$
$$C_7^{(2)}(x) = \frac{x}{12}\left\{\frac{-5x^2+8x-3+(6x-4)\ln x}{(x-1)^3}\right\},$$
$$C_8^{(1)}(x) = \frac{x}{24}\left\{\frac{-x^3+6x^2-3x-2-6x\ln x}{(x-1)^4}\right\},$$
$$C_8^{(2)}(x) = \frac{x}{4}\left\{\frac{-x^2+4x-3-2\ln x}{(x-1)^3}\right\}. \tag{4.28}$$

Here $\lambda^{H^-}_{t_{L,R}}$ are given by Eqs. (3.31) and (3.32). The Wilson coefficients in the SM at one loop are given by $C_7^{\rm SM} = 3C_7^{(1)}(m_t^2/m_W^2)$ and $C_8^{\rm SM} = 3C_8^{(1)}(m_t^2/m_W^2)$. $C_8^{\rm BSM}$ mixes into the $C_7^{\rm BSM}$ at the scale of $\mu_b = m_b$ through the renormalization group equations and contribute to $\mathcal{B}(B \to X_s\gamma)$ [48]. The next-to-next-leading order SM prediction for $\mathcal{B}(B \to X_s\gamma)$ is [49,50]

$$\mathcal{B}(B \to X_s\gamma) = (3.36 \pm 0.23) \times 10^{-4}, \tag{4.29}$$

whereas the experimentally measured value of $\mathcal{B}(B \to X_s\gamma)$ from HFAG is [45]

$$\mathcal{B}(B \to X_s\gamma) = (3.43 \pm 0.21 \pm 0.07) \times 10^{-4}. \tag{4.30}$$

As a result, the SM prediction for $B \to X_s\gamma$ is consistent with experiments, so we obtain the bounds on the modified Wilson coefficients as $-0.032 < C_7^{\rm BSM}(\mu_b) < 0.027$ at 2σ level [51]. This constrains $\tan\beta$ in terms of charged Higgs mass as shown in Fig. 5, where unitarity and stability bounds are displayed as well. We also find that the case with $y^u_{33} = y_t^{\rm SM}/\cos\beta$ has been excluded by $B \to X_s\gamma$, hence the case with $y^u_{33} = y_t^{\rm SM}$ is considered in Figs. 4 and 5 and collider studies in the next section.

4.5 Predictions for R_D and R_{D^*}

We briefly discuss the implications of flavor-violating couplings with charged Higgs on R_D and R_{D^*}. The effective Hamiltonian relevant for $B \to D^{(*)}\tau\nu$ in our model is given as follows:

$$\mathcal{H}_{\rm eff} = C^{cb}_{\rm SM}(\bar{c}_L\gamma_\mu b_L)(\bar{\tau}_L\gamma^\mu\nu_L) + C^{cb}_R(\bar{c}_L b_R)(\bar{\tau}_R\nu_L) + C^{cb}_L(\bar{c}_R b_L)(\bar{\tau}_R\nu_L), \tag{4.31}$$

where the Wilson coefficient in the SM is $C^{cb}_{\rm SM} = 2V_{cb}/v^2$, and the new Wilson coefficients generated by charged Higgs exchanges are

$$C^{cb}_R = -\frac{\sqrt{2}m_\tau\tan\beta}{v\,m^2_{H^\pm}}(\lambda^{H^-}_{c_L})^*,$$
$$C^{cb}_L = -\frac{\sqrt{2}m_\tau\tan\beta}{v\,m^2_{H^\pm}}(\lambda^{H^-}_{c_R})^*. \tag{4.32}$$

See Eqs. (3.33) and (3.34) for $\lambda^{H^-}_{c_{L,R}}$.

The ratios of the branching ratios for $B \to D^{(*)}\tau\nu$ to $B \to D^{(*)}\ell\nu$ with $\ell = e, \mu$ are defined by

$$R_{D^{(*)}} = \frac{\mathcal{B}(B \to D^{(*)}\tau\nu)}{\mathcal{B}(B \to D^{(*)}\ell\nu)}. \tag{4.33}$$

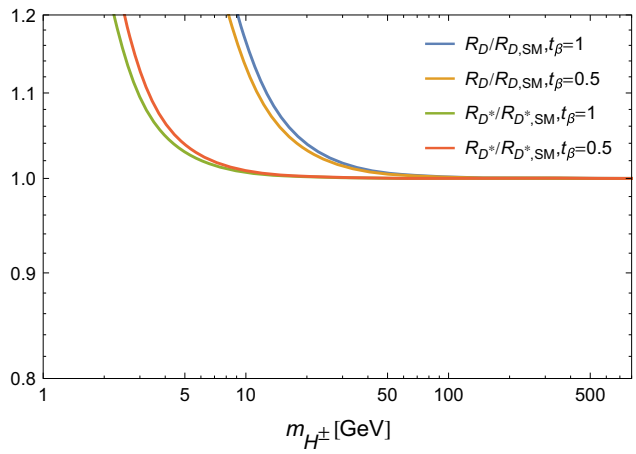

Fig. 6 The ratios of $R_D/R_{D,\mathrm{SM}}$ and $R_{D^*}/R_{D^*,\mathrm{SM}}$ as the functions of charged Higgs mass for given $\tan\beta$

The SM expectations are $R_D = 0.300 \pm 0.008$ and $R_{D^*} = 0.252 \pm 0.003$ [52], but the experimental results for $R_{D^{(*)}}$ are deviated from the SM values by more than 2σ [7–11]. Including the additional contributions from charged Higgs exchanges, we find the simplified forms for R_D and R_{D^*} as follows [47,53]:

$$R_D = R_{D,\mathrm{SM}}\left[1 + 1.5\,\mathrm{Re}\left(\frac{C_R^{cb}+C_L^{cb}}{C_{\mathrm{SM}}^{cb}}\right) + \left|\frac{C_R^{cb}+C_L^{cb}}{C_{\mathrm{SM}}^{cb}}\right|^2\right],$$
$$R_{D^*} = R_{D^*,\mathrm{SM}}\left[1 + 0.12\,\mathrm{Re}\left(\frac{C_R^{cb}-C_L^{cb}}{C_{\mathrm{SM}}^{cb}}\right) + 0.05\left|\frac{C_R^{cb}-C_L^{cb}}{C_{\mathrm{SM}}^{cb}}\right|^2\right]. \tag{4.34}$$

As can be seen in Fig. 6, a light charged Higgs is necessary to have large deviations of R_D and R_{D^*}. However, it is excluded by $B \to X_s\gamma$. [See Fig. 5]. Therefore, our model cannot explain the experimental results for $R_{D^{(*)}}$ simultaneously with the other bounds.

5 Productions and decays of heavy Higgs bosons at the LHC

We investigate the main production channels for heavy Higgs bosons at the LHC, including the contributions from flavor-violating interactions of quarks. The decay modes of the heavy Higgs bosons for some benchmark points are also studied, and we discuss smoking gun signals for heavy Higgs searches at the LHC. In this section, mixings with singlet scalar have been neglected and the heavy neutral Higgs boson H denotes h_2. $h \equiv h_1$ is the SM-like Higgs with $m_h = 125$ GeV.

5.1 Heavy neutral Higgs boson

The main channels for neutral Higgs productions are the gluon fusion $gg \to H$, bottom-quark fusion $b\bar{b} \to H$, and additional productions through the flavor-violating interactions for the bottom quark, $b\bar{d}_i \to H$ and $d_i\bar{b} \to H$, where d_i denotes light down-type quarks, $d_i = d,\ s$. There are bottom quark associated productions, $bg \to bH$ and $d_i g \to bH$, as well.

The leading-order cross section for the gluon fusion process at parton level is

$$\hat{\sigma}(gg \to H) = \frac{\alpha_s^2 m_H^2}{576\pi v^2} \times \left|\frac{3}{4}\sum_q\left(\frac{\cos\alpha}{\cos\beta} + \frac{v\sin(\alpha-\beta)}{\sqrt{2}m_q\cos\beta}\tilde{h}_{33}^q\right)A_{1/2}^H(\tau_q)\right|^2 \times\delta(\hat{s}-m_H^2), \tag{5.1}$$

where $\tau_q = m_H^2/(4m_q^2)$. The loop function $A_{1/2}^H(\tau)$ is given in Ref. [54]. $\hat{s}$ is the partonic center-of-mass energy. Here the contributions of only top and bottom quarks have been taken into account. Note that the top quark contribution is vanishing if one takes $y_{33}^u = y_t^{\mathrm{SM}}$ and the alignment limit as can be seen in Eq. (3.37). The parton-level cross section for bottom-quark fusion $b\bar{b} \to H$ is

$$\hat{\sigma}(b\bar{b} \to H) = \frac{\pi m_b^2}{18v^2}\left(\frac{\cos\alpha}{\cos\beta} + \frac{v\sin(\alpha-\beta)}{\sqrt{2}m_b\cos\beta}\tilde{h}_{33}^d\right)^2 \times\left(1-\frac{4m_b^2}{m_H^2}\right)^{1/2}\delta(\hat{s}-m_H^2). \tag{5.2}$$

There are other single Higgs production channels through the flavor-violating interactions, $b\bar{d}_i \to H$ and $d_i\bar{b} \to H$. The corresponding cross section is given by

$$\hat{\sigma}(d_i\bar{b} \to H) = \frac{\pi|\tilde{h}_{i3}^d|^2\sin^2(\alpha-\beta)}{72\cos^2\beta}\delta(\hat{s}-m_H^2), \tag{5.3}$$

and $\hat{\sigma}(b\bar{d}_i \to H) = \hat{\sigma}(d_i\bar{b} \to H)$ at parton level.

The bottom quark associated production of the Higgs boson can occur by initial states with a bottom quark, that is, $bg \to bH$, through the flavor-conserving interactions or initial states with a light down-type quark, $d_i g \to bH$, via the flavor-violating interactions. The former is nonvanishing even if all the components of $\tilde{h}^d$ are zero. The diagrams of the bottom quark associated production are shown in Fig. 7. The differential cross section for $bg \to bH$ at parton level is

$$\frac{d\hat{\sigma}}{d\hat{t}}(bg \to bH) = \frac{\alpha_s(\lambda_b^H)^2}{96(\hat{s}-m_b^2)^2}\left[\frac{2F_1 - F_2^2 - 2G_1G_2}{(\hat{s}-m_b^2)(\hat{t}-m_b^2)} + 2m_b^2\left(\frac{G_1}{(\hat{s}-m_b^2)^2} + \frac{G_2}{(\hat{t}-m_b^2)^2}\right)\right], \tag{5.4}$$

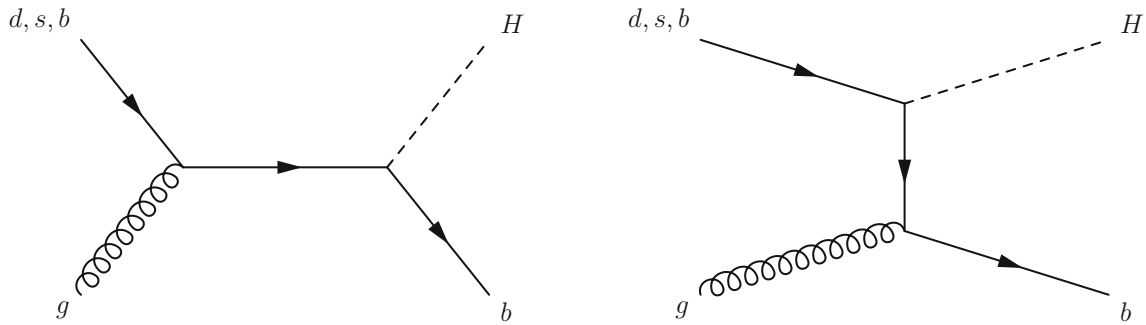

Fig. 7 Diagrams of the bottom quark associated productions of neutral Higgs bosons

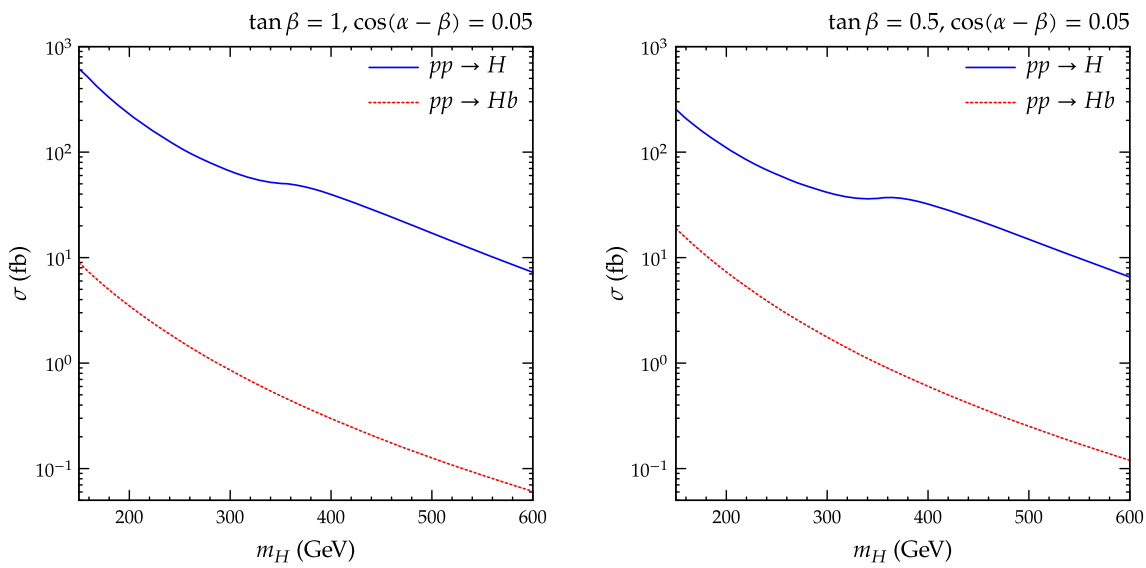

Fig. 8 Production cross sections of the heavy neutral Higgs H at 14 TeV proton-proton collisions. We have chosen $\tan\beta = 1$ (left panel) and $\tan\beta = 0.5$ (right panel) with $\cos(\alpha-\beta) = 0.05$ and $y^u_{33} = y_t^{\rm SM}$

where

$$F_1 = \hat{s}\hat{t} - m_b^4, \quad F_2 = \hat{s} + \hat{t} - 2m_b^2,$$
$$G_1 = m_H^2 - m_b^2 - \hat{s}, \quad G_2 = m_H^2 - m_b^2 - \hat{t},$$

and λ_b^H is given in (3.22). For the $d_i g \to bH$ process, it is

$$\frac{d\hat{\sigma}}{d\hat{t}}(d_i g \to bH) = \frac{\alpha_s |\tilde{h}^d_{i3}|^2}{96\hat{s}^2(\hat{t} - m_b^2)} \frac{\sin^2(\alpha-\beta)}{\cos^2\beta} \times \left[\frac{2F_1 - F_2^2 - 2G_1G_2}{\hat{s}} + \frac{2m_b^2 G_2}{\hat{t} - m_b^2}\right] \tag{5.5}$$

with

$$F_1 = \hat{s}\hat{t}, \;\; F_2 = \hat{s} + \hat{t} - m_b^2, \;\; G_1 = m_H^2 - m_b^2 - \hat{s}, \;\; G_2 = m_H^2 - \hat{t}.$$

And again, $\hat{\sigma}(\bar{d}_i g \to \bar{b}H) = \hat{\sigma}(d_i g \to bH)$ at parton level.

We perform the integration by using the Monte Carlo method to obtain the production cross sections at proton-proton collisions of 14 TeV and employ the NNPDF2.3 parton distribution function (PDF) set [55] via the LHAPDF 6 library [56]. The renormalization and factorization scales are set to m_H, and $m_b = 4.7$ GeV. The resulting production cross sections as a function of m_H are shown in Fig. 8. In all frames we set $\cos(\alpha-\beta) = 0.05$, close to the alignment limit, and $y^u_{33} = y_t^{\rm SM}$. A constant K-factor of 2.5 has been multiplied to the gluon fusion production cross section, while the leading-order expressions have been used for the other production channels.

In the alignment limit, the neutral Higgs coupling to the top quarks λ_t^H is vanishing as can be seen in Eq. (3.37). In this case, the single Higgs production through the gluon fusion process is suppressed compared to the SM case, though nonvanishing due to the bottom quarks in the loop. Still, the gluon fusion production convoluted with PDF is the most dominant channel for the single Higgs production and $b\bar{b} \to H$ is the subdominant one for $\tan\beta \gtrsim \mathcal{O}(0.1)$. On the other hand, for smaller $\tan\beta$, the flavor-violating Higgs couplings to light quarks become larger and contribu-

tions from the initial states with the light down-type quarks $d_i\bar{b} \to H$ is subdominant, and become even the most dominant channel in the case of very small $\tan\beta = \mathcal{O}(0.01)$. However, since we find that such scenarios with very small $\tan\beta$ have been excluded by bounds from the experimental results on B-meson mixings and decays, particularly by $B \to X_s\gamma$ as seen in the previous section, we have chosen $\tan\beta = 1$ and 0.5 as benchmarks for this study. For $m_H = 200$ GeV and $\tan\beta = 1$ (0.5), $\sigma_{pp\to H} \simeq 225.2$ (110.5) fb, and $(\sigma_{b\bar{d}_i\to H} + \sigma_{d_i\bar{b}\to H})/\sigma_{gg\to H} = 0.62\%$ (1.6%), while $(\sigma_{b\bar{d}_i\to H} + \sigma_{d_i\bar{b}\to H})/\sigma_{b\bar{b}\to H} \simeq 1.6\%$ (10.9%) at the LHC. As the neutral Higgs gets heavier, the production cross sections rapidly decreases. For $m_H = 400$ GeV and $\tan\beta = 1$ (0.5), $\sigma_{pp\to H} \simeq 38.4$ (31.7) fb.

As can be seen in Fig. 8, the production cross section of the bottom quark associated process increases as $\tan\beta$ is smaller since the effect of the flavor-violating couplings become larger. In particular, if $m_H \lesssim 200$ GeV the production cross section is $\mathcal{O}(10)$ fb, so it can be served as a good search channel at the LHC. Meanwhile, if $m_H \gtrsim 2m_t$, the cross section decreases down to $\lesssim \mathcal{O}(1)$ fb.

We now turn to the decay widths of the neutral Higgs bosons and obtain their branching ratios. Ignoring the mixing among the SM-like Higgs and singlet scalar, the partial decay widths to quarks are

$$\begin{aligned}\Gamma(H \to b\bar{d}_i) &= \Gamma(H \to d_i\bar{b}) \\ &= \frac{3|\tilde{h}^d_{i3}|^2 \sin^2(\alpha-\beta)}{32\pi\cos^2\beta} m_H \left(1 - \frac{m_b^2}{m_H^2}\right)^2, \\ \Gamma(H \to q\bar{q}) &= \frac{3(\lambda_q^H)^2}{16\pi} m_H \left(1 - \frac{4m_q^2}{m_H^2}\right)^{3/2}, \end{aligned} \tag{5.6}$$

where $q = t, b, c$. λ_b^H and λ_t^H are given in (3.22) and (3.23), and

$$\lambda_c^H = \frac{\sqrt{2}m_c\cos\alpha}{v\cos\beta}. \tag{5.7}$$

On the other hand, the Higgs interactions to the charged leptons are flavor-conserving and the corresponding decay width is given as

$$\Gamma(H \to \tau^+\tau^-) = \frac{m_\tau^2\cos^2\alpha}{8\pi v^2\cos^2\beta} m_H \left(1 - \frac{4m_\tau^2}{m_H^2}\right)^{3/2}. \tag{5.8}$$

The partial widths to electroweak gauge bosons $V = W$, Z are given as

$$\Gamma(H \to VV) = \frac{\delta_V m_H^3 \cos^2(\alpha-\beta)}{32\pi v^2} \times \left(1 - \frac{4m_V^2}{m_H^2}\right)^{1/2} \left(1 - \frac{4m_V^2}{m_H^2} + \frac{12m_V^4}{m_H^4}\right), \tag{5.9}$$

where $\delta_W = 2$ and $\delta_Z = 1$. These partial widths are vanishing in the alignment limit. If $m_H > 2m_{Z'}$, the decay mode of $H \to Z'Z'$ opens. Ignoring the small mixing with the Z boson, the decay width is

$$\Gamma(H \to Z'Z') = \frac{g_{Z'}^4 x^4 m_H^3 v^2 \sin^2\beta \sin^2\alpha}{2592\pi m_Z^4} \left(1 - \frac{4m_{Z'}^2}{m_H^2}\right)^{1/2} \times \left(1 - \frac{4m_{Z'}^2}{m_H^2} + \frac{12m_{Z'}^4}{m_H^4}\right). \tag{5.10}$$

However, we find that this decay mode is almost negligible for small $g_{Z'}x \simeq \mathcal{O}(0.05)$ and $m_{Z'} \gtrsim 400$ GeV, which would be necessary to evade constraints from the Z' searches at the LHC.

The neutral Higgs boson can also decay into $\gamma\gamma$ and gg through fermion or gauge boson loops. At leading order, the decay widths are given as

$$\begin{aligned}\Gamma(H \to \gamma\gamma) &= \frac{\alpha^2 m_H^3}{256\pi^3 v^2} \left| \sum_{q=t,b} 3Q_q^2 \frac{\lambda_q^H v}{\sqrt{2}m_q} A_{1/2}^H(\tau_q) \right. \\ &\quad \left. + \frac{\cos\alpha}{\cos\beta} A_{1/2}^H(\tau_\tau) + \cos(\alpha-\beta) A_1^H(\tau_W) \right|^2, \\ \Gamma(H \to gg) &= \frac{\alpha_s^2 m_H^3}{72\pi^3 v^2} \left| \frac{3}{4} \sum_{q=t,b} \frac{\lambda_q^H v}{\sqrt{2}m_q} A_{1/2}^H(\tau_q) \right|^2, \end{aligned} \tag{5.11}$$

where Q_q is the electric charge of the quark and $\tau_i \equiv m_H^2/(4m_i^2)$. The loop functions $A_{1/2}^H$ and A_1^H can be found in Ref. [54].

If $m_H > 2m_h$, the heavy neutral Higgs can decay into a pair of SM-like Higgs bosons.[2] The triple interaction comes from the scalar potential in (2.3),

$$V_1 \supset \frac{g_{Hhh} v}{2} Hhh, \tag{5.12}$$

where

$$\begin{aligned} g_{Hhh} = &\ 3(\lambda_1 \sin\alpha\cos\beta + \lambda_2\cos\alpha\sin\beta)\sin(2\alpha) \\ &+ (\lambda_3 + \lambda_4)\left[3\cos(\alpha+\beta)\cos(2\alpha) - \cos(\alpha-\beta)\right]. \end{aligned} \tag{5.13}$$

[2] If the singlet scalar $h_3 = S$ is light enough, additional decay modes such as $H \to Sh$ can occur and become important channels (See, for example, [57,58]). Here we assume that S is heavy, $m_S \gtrsim 0.5$–1 TeV, and the mixings with doublet Higgs bosons are negligible.

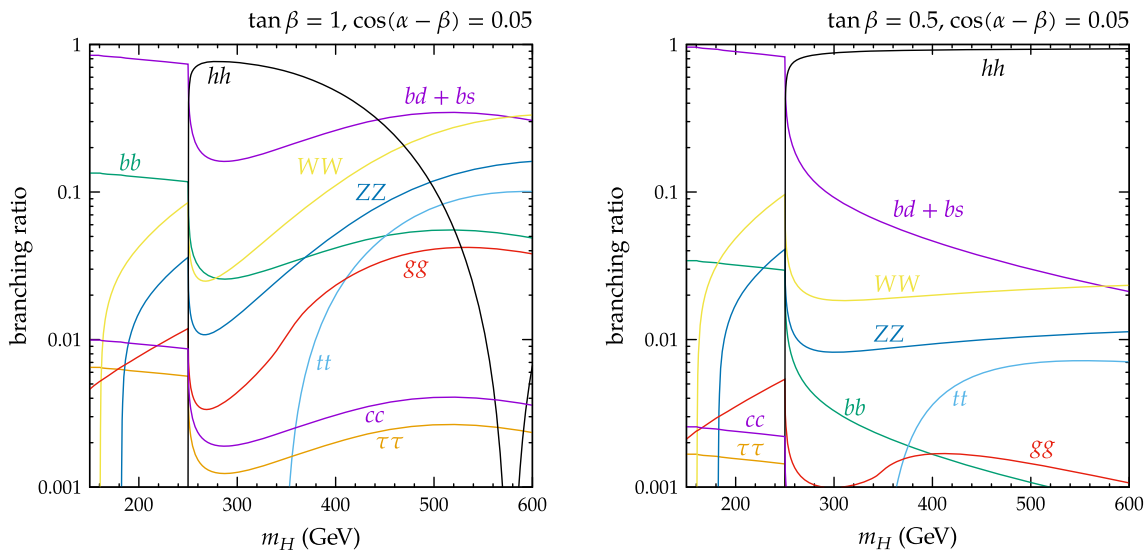

Fig. 9 Branching ratios of the heavy neutral Higgs H. $\tan\beta = 1$ and $\mu = 200$ GeV (left panel), and $\tan\beta = 0.5$ and $\mu = 50$ GeV (right panel) have been taken. $v_s = 1$ TeV and $\cos(\alpha - \beta) = 0.05$ for both panels

The decay width for the $H \to hh$ process is given as

$$\Gamma(H \to hh) = \frac{g_{Hhh}^2 v^2}{32\pi m_H}\left(1 - \frac{4m_h^2}{m_H^2}\right)^{1/2}. \tag{5.14}$$

The quartic couplings in the Higgs potential can be evaluated by choosing values of μv_s, $\tan\beta$, $\sin\alpha$, and m_H if mixing with the singlet scalar is negligible, $\alpha_2 \simeq \alpha_3 \simeq 0$. See Appendix A.

By combining all the decay widths, we obtain the branching ratio of each decay mode. Fig. 9 shows the branching ratios of the neutral Higgs boson H for $\cos(\alpha - \beta) = 0.05$ and $v_s = 1$ TeV, but with different values of μ to satisfy the unitary and stability bounds studied in Sect. 4.1. We observe that $H \to b\bar{d}_i/d_i\bar{b}$ is the predominant decay mode if $m_H < 2m_h$, whereas the di-Higgs mode $H \to hh$ becomes the most important if the mode is kinematically allowed, irrespective of $\tan\beta$. In practice, the branching ratio of di-Higgs mode $\mathcal{B}(H \to hh)$ depends on the choice of μv_s value. If we take a smaller μv_s value, for instance, $\mu = 200$ GeV and $v_s = 500$ GeV with $\tan\beta = 1$, we find that $H \to b\bar{d}_i/d_i\bar{b}$ is always the most dominant decay mode. The dip near $m_H = 580$ GeV in the left panel of Fig. 9 is due to the accidental cancellation in the Higgs triple coupling (5.13). The position of dip also depends on the value of μv_s for given $\tan\beta$ and $\cos(\alpha - \beta)$. On the other hand, the $b\bar{b}$ mode and diboson modes such as WW/ZZ are subdominant.

From these observations, we expect that the search strategies would be different depending on the mass of the heavy Higgs boson. For $m_H < 2m_h$, $pp \to H \to b\bar{d}_i/d_i\bar{b}$, i.e., dijet final states containing one b jet is the most important, but for $m_H > 2m_h$, the di-Higgs channel, and possibly in conjunction with the dijet channel with one b jet, is important to search the heavy neutral Higgs boson at the LHC. Thus, the neutral Higgs boson with $m_H < 250$ GeV can receive constraints from dijet searches [59–61]. Although the dijet channel has typically been used to seek for heavy resonances in a few TeV scales, it can probe lower scales if it is associated with a hard photon or jet from initial state radiations. The ATLAS collaboration has searched light resonance with dijet invariant mass down to 200 GeV in the final states of dijet in association with a photon [62,63]. In our case, gluon fusion production is the most dominant channel and it is not associated with a hard photon. It can have a hard jet from the gluons in the initial states, but the mass region below 250 GeV has not been searched yet in the final states of dijet in association with a hard jet. For $m_H > 250$ GeV, bounds from di-Higgs searches can be imposed, but we find that they do not have enough sensitivities for heavy neutral Higgs bosons in our model yet [64–67].

5.2 Heavy charged Higgs boson

One of the conventional search channels for the heavy charged Higgs with $m_{H^\pm} > m_t$ at hadron colliders is the top quark associated production, $bg \to tH^-$, by the similar diagrams as $bg \to bH$. Since the charged Higgs boson can have enhanced couplings with the light up-type quarks due to nonzero components of $\tilde{h}^d$, we can also have a sizable production cross section of the bottom quark associated process from the initial states with light up-type quarks, $u_i g \to bH^+$ where $u_i = u, c$.[3]

[3] We note that there have been collider studies on the production of heavy Higgs bosons due to flavor-violating interactions for up-type quarks. See, for instance, Refs. [17,18].

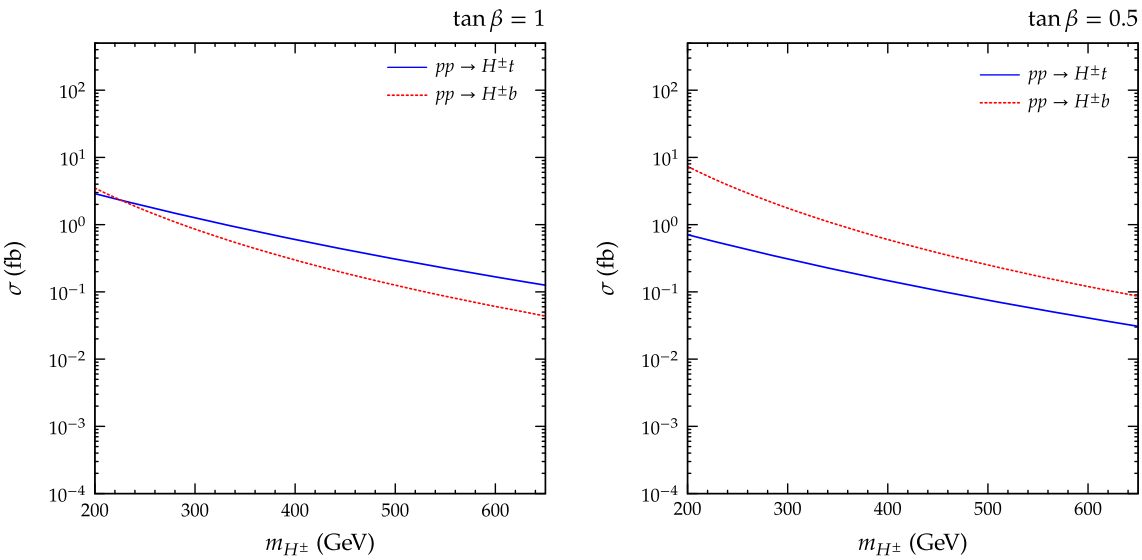

Fig. 10 Production cross sections of the heavy charged Higgs $H^{\pm}$ at 14 TeV proton-proton collisions. We have chosen $\tan\beta = 1$ (left panel) and $\tan\beta = 0.5$ (right panel) with $y^u_{33} = y_t^{\rm SM}$

The differential cross section for $bg \to tH^-$ at parton level is

$$\frac{d\hat{\sigma}}{d\hat{t}} = \frac{\alpha_s}{48(\hat{s}-m_b^2)^2}\Bigg[\left(|\lambda^{H^-}_{t_L}|^2 + |\lambda^{H^-}_{t_R}|^2\right) \times \left(\frac{2F_1 - F_2^2 - 2G_1G_2}{(\hat{s}-m_b^2)(\hat{t}-m_t^2)} + \frac{2m_b^2G_1}{(\hat{s}-m_b^2)^2} + \frac{2m_t^2G_2}{(\hat{t}-m_t^2)^2}\right) + \left(\lambda^{H^-}_{t_L}(\lambda^{H^-}_{t_R})^* + \lambda^{H^-}_{t_R}(\lambda^{H^-}_{t_L})^*\right)\frac{4m_bm_tm^2_{H^\pm}}{(\hat{s}-m_b^2)(\hat{t}-m_t^2)} \times \left(1 - \frac{F_1F_2}{m^2_{H^\pm}(\hat{s}-m_b^2)(\hat{t}-m_t^2)}\right)\Bigg], \tag{5.15}$$

where

$$F_1 = \hat{s}\hat{t} - m_b^2m_t^2, \quad F_2 = \hat{s} + \hat{t} - m_b^2 - m_t^2,$$
$$G_1 = m^2_{H^\pm} - m_t^2 - \hat{s}, \quad G_2 = m^2_{H^\pm} - m_b^2 - \hat{t}. \tag{5.16}$$

Since the diagrams contributing to bottom quark associated processes has the same Lorentz structure as those for $bg \to tH^-$, we can obtain their parton-level cross sections by replacing $\lambda^{H^-}_{t_{L,R}}$ with $\lambda^{H^-}_{u_{iL,R}}$, m_b with $m_{u_i} \simeq 0$, and m_t with m_b. They are given as

$$\frac{d\hat{\sigma}}{d\hat{t}}(u_ig \to bH^+) = \frac{\alpha_s(|\lambda^{H^-}_{u_{iL}}|^2 + |\lambda^{H^-}_{u_{iR}}|^2)}{48\hat{s}^2(\hat{t}-m_b^2)} \times \left[\frac{2F_1 - F_2^2 - 2G_1G_2}{\hat{s}} + \frac{2m_b^2G_2}{\hat{t}-m_b^2}\right] \tag{5.17}$$

with

$$F_1 = \hat{s}\hat{t}, \quad F_2 = \hat{s} + \hat{t} - m_b^2, \quad G_1 = m^2_{H^\pm} - m_b^2 - \hat{s},$$
$$G_2 = m^2_{H^\pm} - \hat{t}. \tag{5.18}$$

The leading-order cross sections evaluated by convoluting the partonic cross section with the PDFs at proton-proton collisions of 14 TeV are shown in Fig. 10. In each figure, $\sigma(pp \to H^\pm q) = \sigma(pp \to H^+q) + \sigma(pp \to H^-q)$. The production cross sections are quite sensitive to $\tan\beta$. For $\tan\beta = 1$, the top quark associated production, $pp \to H^\pm t$, is the dominant channel, while the bottom quark associated production, $pp \to H^\pm b$, which is the characteristic channel of our model, can also be served as a good channel to search the charged Higgs boson at the LHC. On the other hand, for smaller $\tan\beta$, the bottom quark associated production becomes the dominant channel due to the enhanced charged-Higgs couplings with light up-type quarks. The suppression of top quark associated production is also due to the partial cancellation of two terms in $\lambda^{H^-}_{t_L}$.

Concerning the decays of charged Higgs, the most important fermionic decay mode is $H^+ \to t\bar{b}$. The decay width is

$$\Gamma(H^+ \to t\bar{b}) = \Gamma(H^- \to b\bar{t}) = \frac{3}{16\pi}m_{H^\pm}\left[\left(1 - \frac{(m_t+m_b)^2}{m^2_{H^\pm}}\right)\left(1 - \frac{(m_t-m_b)^2}{m^2_{H^\pm}}\right)\right]^{1/2} \times \left[\left(|\lambda^{H^-}_{t_L}|^2 + |\lambda^{H^-}_{t_R}|^2\right)\left(1 - \frac{m_t^2+m_b^2}{m^2_{H^\pm}}\right) - 2\left(\lambda^{H^-}_{t_L}(\lambda^{H^-}_{t_R})^* + \lambda^{H^-}_{t_R}(\lambda^{H^-}_{t_L})^*\right)\frac{m_tm_b}{m^2_{H^\pm}}\right]. \tag{5.19}$$

By replacing m_t with m_c or m_u and $\lambda^{H^-}_{t_{L,R}}$ with $\lambda^{H^-}_{c_{L,R}}$ or $\lambda^{H^-}_{u_{L,R}}$, one can obtain the decay widths of $H^+ \to c\bar{b}$ and

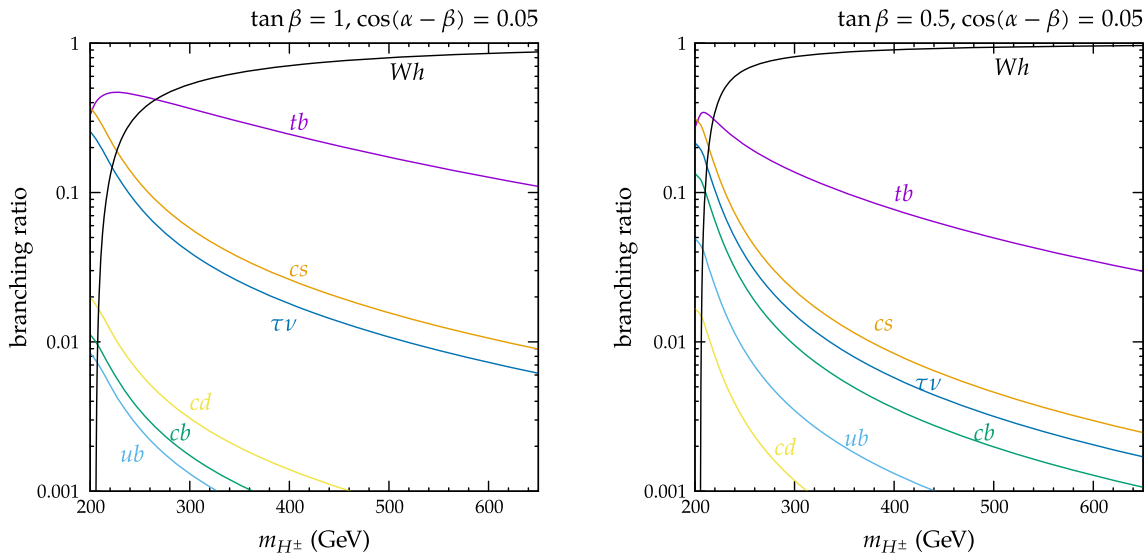

Fig. 11 Branching ratios of the heavy charged Higgs $H^{\pm}$. $\tan\beta = 1$ (left panel) and $\tan\beta = 0.5$ (right panel) have been taken. $\cos(\alpha-\beta) = 0.05$ and $y^u_{33} = y_t^{\rm SM}$ for both panels

$H^+ \to u\bar{b}$. The other fermionic decay modes are $H^+ \to c\bar{s}$ and $c\bar{d}$, whose decay widths are proportional to $\tan^2\beta|V_{cs}|^2$ and $\tan^2\beta|V_{cd}|^2$, respectively. The decay widths of leptonic decay modes are given as

$$\Gamma(H^+ \to \ell^+\nu) = \Gamma(H^- \to \ell^-\bar{\nu}) = \frac{m_\ell^2 \tan^2\beta}{8\pi v^2} m_{H^\pm}\left(1 - \frac{m_\ell^2}{m_{H^\pm}^2}\right)^2 . \quad (5.20)$$

Meanwhile, if $H^+ \to W^+A$ and W^+H are kinematically forbidden, the only non-fermionic decay mode is $H^+ \to W^+h$. The decay width is

$$\Gamma(H^+ \to W^+h) = \Gamma(H^- \to W^-h) = \frac{g^2\cos^2(\alpha-\beta)m_{H^\pm}^3}{64\pi m_W^2} \times \left[\left(1 - \frac{m_W^2}{m_{H^\pm}^2} - \frac{m_h^2}{m_{H^\pm}^2}\right)^2 - \frac{4m_W^2 m_h^2}{m_{H^\pm}^4}\right]^{3/2} . \quad (5.21)$$

By combining all the decay modes in the above we obtain the branching ratios of the heavy charged Higgs, which are shown in Fig. 11. Interestingly, the dominant decay mode of the charged Higgs boson is $H^+ \to W^+h$ if it is kinematically allowed, although we have taken the alignment limit. $H^+ \to t\bar{b}$ is subdominant. Together with the production, we expect that $pp \to H^\pm b \to W^\pm h + b$ can be served as the important process to probe the charged Higgs boson at the LHC and future hadron colliders. Most LHC searches for W^+h have been dedicated to heavy resonances [68–70] that decay directly into W^+h, so our model is not constrained by W^+h at the moment. On the other hand, the $t\bar{b}$ mode is next-to-dominant and this is not constrained by the current LHC data [71,72], because the production cross section for the heavy charged Higgs in our model is less than 10 fb in most of the parameter space.

6 Conclusions

We have considered an extra local $U(1)$ with flavor-dependent couplings as a linear combination of $B_3 - L_3$ and $L_\mu - L_\tau$, that has been recently proposed to explain the B-meson anomalies. In our model, we have reproduced the correct flavor structure of the quark sector due to the VEV of the second Higgs doublet, at the expense of new flavor violating couplings for quarks and the violation of lepton universality.

The extra gauge boson leads to flavor violating interactions for down-type quarks appropriate for explaining B-meson anomalies in $R_{K^{(*)}}$ whereas heavy Higgs bosons render up-type quarks have modified flavor-conserving Yukawa couplings and down-type quarks receive flavor-violating Yukawa couplings. We also found that the B-meson anomalies in $R_{D^{(*)}}$ cannot be explained by the charged Higgs boson in our model, due to small flavor-violating couplings.

We showed how the extended Higgs sector can be constrained by unitarity and stability, Higgs and electroweak precision data, B-meson decays/mixings. Taking the alignment limit of heavy Higgs bosons from Higgs precision data, we also investigated the production of heavy Higgs bosons at the LHC. We found that there are reductions in the cross sections of the usual production channels in 2HDM, such as $pp \to H$ and $pp \to H^\pm t$ at the LHC. In addition, new

production channels such as $pp \to Hb$ and $pp \to H^{\pm}b$ become important for $\tan\beta \lesssim 1$. Decay products of heavy Higgs bosons lead to interesting collider signatures due to large branching fractions of $bd + bs$ modes for neutral Higgs bosons and $W^{\pm}h$ mode for charged Higgs boson if kinematically allowed, thus requiring a more dedicated analysis for the LHC.

Acknowledgements The work is supported in part by Basic Science Research Program through the National Research Foundation of Korea (NRF) funded by the Ministry of Education, Science and Technology (NRF-2016R1A2B4008759). The work of LGB is partially supported by the National Natural Science Foundation of China (under Grant no. 11605016), Korea Research Fellowship Program through the National Research Foundation of Korea (NRF) funded by the Ministry of Science and ICT (2017H1D3A1A01014046). The work of CBP is supported by IBS under the project code, IBS-R018-D1.

Appendix A: The extended Higgs sector

By using the minimization condition of the Higgs potential given by

$$\mu_1^2 = \frac{\sqrt{2}\mu v_2 v_s - 2\lambda_1 v_1^3 - 2\lambda_3 v_1 v_2^2 - 2\lambda_4 v_1 v_2^2 - 2\kappa_1 v_1 v_s^2}{2v_1},$$

$$\mu_2^2 = \frac{\sqrt{2}\mu v_1 v_s - 2\lambda_3 v_1^2 v_2 - 2\lambda_4 v_1^2 v_2 - 2\lambda_2 v_2^3 - 2\kappa_2 v_2 v_s^2}{2v_2},$$

$$m_s^2 = \frac{\sqrt{2}\mu v_1 v_2 - 2\kappa_1 v_1^2 v_s - 2\kappa_2 v_2^2 v_s - 2\lambda_S v_s^3}{2v_s}, \tag{A.1}$$

the mass matrix for CP-even scalars can be written as

$$M_S = \begin{pmatrix} 2\lambda_1 v_1^2 + \frac{\mu v_2 v_s}{\sqrt{2}v_1} & 2v_1 v_2(\lambda_3+\lambda_4) - \frac{\mu v_s}{\sqrt{2}} & 2\kappa_1 v_1 v_s - \frac{\mu v_2}{\sqrt{2}} \\ 2v_1 v_2(\lambda_3+\lambda_4) - \frac{\mu v_s}{\sqrt{2}} & 2\lambda_2 v_2^2 + \frac{\mu v_1 v_s}{\sqrt{2}v_2} & 2\kappa_2 v_2 v_s - \frac{\mu v_1}{\sqrt{2}} \\ 2\kappa_1 v_1 v_s - \frac{\mu v_2}{\sqrt{2}} & 2\kappa_2 v_2 v_s - \frac{\mu v_1}{\sqrt{2}} & 2\lambda_S v_s^2 + \frac{\mu v_1 v_2}{\sqrt{2}v_s} \end{pmatrix}. \tag{A.2}$$

We introduce a rotation matrix R to change the interaction basis (ρ_1, ρ_2, S_R) to the physical mass eigenstates, h_1, h_2 and h_3 as

$$\begin{pmatrix} h_1 \\ h_2 \\ h_3 \end{pmatrix} = R \begin{pmatrix} \rho_1 \\ \rho_2 \\ S_R \end{pmatrix}.$$

The mass matrix M_S can be then diagonalized as

$$R M_S R^{\mathsf{T}} = \mathrm{diag}(m_{h_1}^2, m_{h_2}^2, m_{h_3}^2). \tag{A.3}$$

We use a convention such that the mass eigenstates are ordered as $m_{h_1} < m_{h_2} < m_{h_3}$. Here, the orthogonal matrix R is parametrized in terms of the mixing angles α_1 to α_3 as

$$R = \begin{pmatrix} c_{\alpha_1}c_{\alpha_2} & s_{\alpha_1}c_{\alpha_2} & s_{\alpha_2} \\ -(c_{\alpha_1}s_{\alpha_2}s_{\alpha_3} + s_{\alpha_1}c_{\alpha_3}) & c_{\alpha_1}c_{\alpha_3} - s_{\alpha_1}s_{\alpha_2}s_{\alpha_3} & c_{\alpha_2}s_{\alpha_3} \\ -c_{\alpha_1}s_{\alpha_2}c_{\alpha_3} + s_{\alpha_1}s_{\alpha_3} & -(c_{\alpha_1}s_{\alpha_3} + s_{\alpha_1}s_{\alpha_2}c_{\alpha_3}) & c_{\alpha_2}c_{\alpha_3} \end{pmatrix}, \tag{A.4}$$

where $s_{\alpha_i} \equiv \sin\alpha_i$ and $c_{\alpha_i} \equiv \cos\alpha_i$. Without loss of generality the angles can be chosen in the range of

$$-\frac{\pi}{2} \le \alpha_{1,2,3} < \frac{\pi}{2}.$$

In the text we focus mainly on the situation where mixings between $\rho_{1,2}$ and S_R are small.

The mass eigenvalues of CP-even neutral scalars are given by

$$\begin{aligned} m_{h_1}^2 &= \frac{1}{2}(a + b - \sqrt{D}) \equiv m_h^2, \\ m_{h_2}^2 &= \frac{1}{2}(a + b + \sqrt{D}) \equiv m_H^2, \\ m_{h_3}^2 &= 2\lambda_S v_s^2 + \frac{\mu v_1 v_2}{\sqrt{2}v_s} \equiv m_s^2, \end{aligned} \tag{A.5}$$

where

$$a \equiv 2\lambda_1 v_1^2 + \frac{\mu v_2 v_s}{\sqrt{2}v_1}, \quad b \equiv 2\lambda_2 v_2^2 + \frac{\mu v_1 v_s}{\sqrt{2}v_2}, \quad D \equiv (a-b)^2 + 4d^2 \tag{A.6}$$

with $d \equiv 2v_1 v_2(\lambda_3 + \lambda_4) - \mu v_s/\sqrt{2}$. We can trade off quartic couplings, $\lambda_{1,2,3,4}$ and $\kappa_{1,2}$, for mixing angles and Higgs masses.

$$\begin{aligned} \lambda_1 &= \frac{2\sum_i m_{h_i}^2 R_{i1}^2 - \sqrt{2}\mu v_s \tan\beta}{4v^2\cos^2\beta}, \\ \lambda_2 &= \frac{2\sum_i m_{h_i}^2 R_{i2}^2 - \sqrt{2}\mu v_s \cot\beta}{4v^2\sin^2\beta}, \\ \lambda_3 + \lambda_4 &= \frac{\sqrt{2}\mu v_s + 2\sum_i m_{h_i}^2 R_{i1}R_{i2}}{4v^2\sin 2\beta}, \\ \lambda_S &= \frac{2v_s\sum_i m_{h_i}^2 R_{i3}^2 - \sqrt{2}\mu v^2 \sin\beta\cos\beta}{4v_s^3}, \\ \kappa_1 &= \frac{\sqrt{2}\mu v \sin\beta + 2\sum_i m_{h_i}^2 R_{i1}R_{i3}}{4vv_s\cos\beta}, \\ \kappa_2 &= \frac{\sqrt{2}\mu v \cos\beta + 2\sum_i m_{h_i}^2 R_{i2}R_{i3}}{4vv_s\sin\beta}. \end{aligned} \tag{A.7}$$

In the case when the Higgs mixings with the singlet scalar are negligible, $\alpha_2 \simeq \alpha_3 \simeq 0$, the rotation matrix can be simplified as

$$R \approx \begin{pmatrix} \cos\alpha & \sin\alpha & 0 \\ -\sin\alpha & \cos\alpha & 0 \\ 0 & 0 & 1 \end{pmatrix}, \tag{A.8}$$

where $\alpha = \alpha_1$. Then the Higgs quartic couplings are given by

$$\lambda_1 \approx \frac{2(m_h^2\cos^2\alpha + m_H^2\sin^2\alpha) - \sqrt{2}\mu v_s \tan\beta}{4v^2\cos^2\beta},$$
$$\lambda_2 \approx \frac{2(m_h^2\sin^2\alpha + m_H^2\cos^2\alpha) - \sqrt{2}\mu v_s \cot\beta}{4v^2\sin^2\beta},$$
$$\lambda_3 + \lambda_4 \approx \frac{(m_h^2 - m_H^2)\sin 2\alpha + \sqrt{2}\mu v_s}{4v^2\sin 2\beta}. \tag{A.9}$$

Here $h = h_1$ with $m_h = 125$ GeV and $H = h_2$. This relations show that the values of quartic couplings can be evaluated solely by m_H if one chooses a benchmark point in terms of μv_s, $\tan\beta$, and $\sin\alpha$.

Appendix B: Unitarity bounds

The initial scattering states can be classified by hypercharges and isospins [73–75]. In the basis of $(\phi_1^+\phi_1^-, \phi_2^+\phi_2^-, \eta_1\eta_1/\sqrt{2}, \rho_1\rho_1/\sqrt{2}, \eta_2\eta_2/\sqrt{2}, \rho_2\rho_2/\sqrt{2}, S_R S_R/\sqrt{2}, S_I S_I/\sqrt{2})$, the scattering amplitude is

$$\mathcal{M}_1 = \begin{pmatrix} 4\lambda_1 & 2(\lambda_3+\lambda_4) & \sqrt{2}\lambda_1 & \sqrt{2}\lambda_1 & \sqrt{2}\lambda_3 & \sqrt{2}\lambda_3 & \sqrt{2}\kappa_1 & \sqrt{2}\kappa_1 \\ 2(\lambda_3+\lambda_4) & 4\lambda_2 & \sqrt{2}\lambda_3 & \sqrt{2}\lambda_3 & \sqrt{2}\lambda_2 & \sqrt{2}\lambda_2 & \sqrt{2}\kappa_2 & \sqrt{2}\kappa_2 \\ \sqrt{2}\lambda_1 & \sqrt{2}\lambda_3 & 3\lambda_1 & \lambda_1 & \lambda_3+\lambda_4 & \lambda_3+\lambda_4 & \kappa_1 & \kappa_1 \\ \sqrt{2}\lambda_1 & \sqrt{2}\lambda_3 & \lambda_1 & 3\lambda_1 & \lambda_3+\lambda_4 & \lambda_3+\lambda_4 & \kappa_1 & \kappa_1 \\ \sqrt{2}\lambda_3 & \sqrt{2}\lambda_2 & \lambda_3+\lambda_4 & \lambda_3+\lambda_4 & 3\lambda_2 & \lambda_2 & \kappa_2 & \kappa_2 \\ \sqrt{2}\lambda_3 & \sqrt{2}\lambda_2 & \lambda_3+\lambda_4 & \lambda_3+\lambda_4 & \lambda_2 & 3\lambda_2 & \kappa_2 & \kappa_2 \\ \sqrt{2}\kappa_1 & \sqrt{2}\kappa_2 & \kappa_1 & \kappa_1 & \kappa_2 & \kappa_2 & 3\lambda_S & \lambda_S \\ \sqrt{2}\kappa_1 & \sqrt{2}\kappa_2 & \kappa_1 & \kappa_1 & \kappa_2 & \kappa_2 & \lambda_S & 3\lambda_S \end{pmatrix}, \tag{B.1}$$

whose eigenvalues are $2\lambda_1, 2\lambda_2, \lambda_1+\lambda_2 \pm \sqrt{(\lambda_1-\lambda_2)^2 + 4\lambda_4^2}$, and $2\lambda_S$.

In the basis of $(\phi_1^+ S_R, \phi_2^+ S_R, \phi_1^+ S_I, \phi_2^+ S_I)$, the submatrix is given by

$$\mathcal{M}_2 = \begin{pmatrix} 2\kappa_1 & 0 & 0 & 0 \\ 0 & 2\kappa_2 & 0 & 0 \\ 0 & 0 & 2\kappa_1 & 0 \\ 0 & 0 & 0 & 2\kappa_2 \end{pmatrix} \tag{B.2}$$

with eigenvalues being $2\kappa_{1,2}$.

In the basis of $(\rho_1\eta_1, \rho_2\eta_2, S_R S_I)$, the matrix is

$$\mathcal{M}_3 = \begin{pmatrix} 2\lambda_1 & 0 & 0 \\ 0 & 2\lambda_2 & 0 \\ 0 & 0 & 2\lambda_S \end{pmatrix} \tag{B.3}$$

with eigenvalues being $2\lambda_{1,2,s}$.

In the basis of $(\phi_1^+\phi_2^-, \phi_2^+\phi_1^-, \rho_1\eta_2, \rho_2\eta_1, \eta_1\eta_2, \rho_1\rho_2)$, we have

$$\mathcal{M}_4 = \begin{pmatrix} 0 & 2\lambda_3+2\lambda_4 & i\lambda_4 & -i\lambda_4 & \lambda_4 & \lambda_4 \\ 2\lambda_3+2\lambda_4 & 0 & -i\lambda_4 & i\lambda_4 & \lambda_4 & \lambda_4 \\ i\lambda_4 & -i\lambda_4 & 2\lambda_3+2\lambda_4 & 0 & 0 & 0 \\ -i\lambda_4 & i\lambda_4 & 0 & 2\lambda_3+2\lambda_4 & 0 & 0 \\ \lambda_4 & \lambda_4 & 0 & 0 & 2\lambda_3+2\lambda_4 & 0 \\ \lambda_4 & \lambda_4 & 0 & 0 & 0 & 2\lambda_3+2\lambda_4 \end{pmatrix} \tag{B.4}$$

with eigenvalues being $2\lambda_3$, $2(\lambda_3+\lambda_4)$, $2(\lambda_3+2\lambda_4)$, and $\pm 2\sqrt{\lambda_3(\lambda_3+2\lambda_4)}$.

Finally, in the basis of $(\rho_1\phi_1^+, \rho_2\phi_1^+, \eta_1\phi_1^+, \eta_2\phi_1^+, \rho_1\phi_2^+, \rho_2\phi_2^+, \eta_1\phi_2^+, \eta_2\phi_2^+)$, we obtain the matrix as

$$\mathcal{M}_5 = \begin{pmatrix} 2\lambda_1 & 0 & 0 & 0 & 0 & \lambda_4 & 0 & i\lambda_4 \\ 0 & 2\lambda_3 & 0 & 0 & \lambda_4 & 0 & -i\lambda_4 & 0 \\ 0 & 0 & 2\lambda_1 & 0 & 0 & -i\lambda_4 & 0 & \lambda_4 \\ 0 & 0 & 0 & 2\lambda_3 & i\lambda_4 & 0 & \lambda_4 & 0 \\ 0 & \lambda_4 & 0 & -i\lambda_4 & 2\lambda_3 & 0 & 0 & 0 \\ \lambda_4 & 0 & i\lambda_4 & 0 & 0 & 2\lambda_2 & 0 & 0 \\ 0 & i\lambda_4 & 0 & \lambda_4 & 0 & 0 & 2\lambda_3 & 0 \\ -i\lambda_4 & 0 & \lambda_4 & 0 & 0 & 0 & 0 & 2\lambda_2 \end{pmatrix}, \tag{B.5}$$

with eigenvalues being $2\lambda_1$, $2\lambda_2$, $2\lambda_3$, $2(\lambda_3 \pm \lambda_4)$, and $\lambda_1+\lambda_2 \pm \sqrt{(\lambda_1-\lambda_2)^2+4\lambda_4^2}$.

The eigenvalues obtained in the above are constrained by unitarity as

$$\begin{aligned} &|2\lambda_{1,2,3,S}| \le 8\pi, \quad |2\kappa_{1,2}| \le 8\pi, \\ &|2(\lambda_3 \pm \lambda_4)| \le 8\pi, \quad |2(\lambda_3+2\lambda_4)| \le 8\pi, \\ &|2\sqrt{\lambda_3(\lambda_3+2\lambda_4)}| \le 8\pi, \\ &|\lambda_1+\lambda_2 \pm \sqrt{(\lambda_1-\lambda_2)^2+4\lambda_4^2}| \le 8\pi, \\ &a_{1,2,3} \le 8\pi. \end{aligned} \tag{B.6}$$

Here $a_{1,2,3}$ are three other solutions of the following equation:

$$\begin{aligned} &x^3 - 2x^2(3\lambda_1+3\lambda_2+2\lambda_S) \\ &\quad - 4x\left(2\kappa_1^2+2\kappa_2^2-9\lambda_1\lambda_2-6\lambda_1\lambda_S \right. \\ &\quad \left. -6\lambda_2\lambda_S+4\lambda_3^2+4\lambda_3\lambda_4+\lambda_4^2\right) \\ &\quad + 16\left(3\kappa_1^2\lambda_2 - 2\kappa_1\kappa_2(2\lambda_3+\lambda_4)+3\kappa_2^2\lambda_1 \right. \\ &\quad \left. +\lambda_S\left((2\lambda_3+\lambda_4)^2-9\lambda_1\lambda_2\right)\right) = 0. \end{aligned} \tag{B.7}$$

Appendix C: The quark Yukawa couplings

The quark Yukawa couplings in the interaction basis are given by

$$\begin{aligned} -\mathcal{L}_Y^q = &\frac{1}{\sqrt{2}}\bar{u}_L((\rho_1-i\eta_1)y^u+(\rho_2-i\eta_2)h^u)u_R \\ &+\frac{1}{\sqrt{2}}\bar{d}_L((\rho_1+i\eta_1)y^u+(\rho_2+i\eta_2)h^u)d_R \\ &-\bar{d}_L(y^u(\phi_1^+)^*+h^u(\phi_2^+)^*)u_R \\ &+\bar{u}_L(y^d\phi_1^+ + h^d\phi_2^+)d_R + \text{h.c.} \end{aligned} \tag{C.1}$$

In the basis of mass eigenstates the quark Yukawa interactions of the CP-even neutral scalars are

$$-\mathcal{L}_Y^q = (\bar{u}'_L Y^u_{H_i} u'_R + \bar{d}'_L Y^d_{H_i} d'_R)H_i + \text{h.c.}, \tag{C.2}$$

where primed fields are mass eigenstates, and

$$\begin{aligned} Y^u_{H_1} &= -\frac{R_{11}}{v\cos\beta}M_u^D + \frac{R_{11}\tan\beta - R_{12}}{\sqrt{2}}\tilde{h}^u, \\ Y^d_{H_1} &= -\frac{R_{11}}{v\cos\beta}M_u^D + \frac{R_{11}\tan\beta - R_{12}}{\sqrt{2}}\tilde{h}^d, \\ Y^u_{H_2} &= -\frac{R_{21}}{v\cos\beta}M_u^D + \frac{R_{21}\tan\beta - R_{22}}{\sqrt{2}}\tilde{h}^u, \\ Y^d_{H_2} &= -\frac{R_{21}}{v\cos\beta}M_d^D + \frac{R_{21}\tan\beta - R_{22}}{\sqrt{2}}\tilde{h}^d, \\ Y^u_{H_3} &= -\frac{R_{31}}{v\cos\beta}M_u^D + \frac{R_{31}\tan\beta - R_{22}}{\sqrt{2}}\tilde{h}^u, \\ Y^d_{H_3} &= -\frac{R_{31}}{v\cos\beta}M_d^D + \frac{R_{31}\tan\beta - R_{22}}{\sqrt{2}}\tilde{h}^d, \end{aligned} \tag{C.3}$$

Assuming the singlet scalars are decoupled and using Eqs. (3.2) to (3.5), the above quark Yukawa interactions become

$$\begin{aligned} -\mathcal{L}_{q,Y} = &(\bar{u}'_L Y^u_h u'_R + \bar{d}'_L Y^d_h d'_R)h + (\bar{u}'_L Y^u_H u'_R + \bar{d}'_L Y^d_H d'_R)H \\ &+ i(\bar{u}'_L Y^u_A u'_R + \bar{d}'_L Y^d_A d'_R)A^0 \\ &+ \bar{u}'(Y_{2,H^+}P_R + Y_{1,H^+}P_L)d'H^+ + \text{h.c.}, \end{aligned} \tag{C.4}$$

where

$$\begin{aligned} Y^u_h &= -\frac{\sin\alpha}{v\cos\beta}M_u^D + \frac{\cos(\alpha-\beta)}{\sqrt{2}\cos\beta}\tilde{h}^u, \\ Y^d_h &= -\frac{\sin\alpha}{v\cos\beta}M_d^D + \frac{\cos(\alpha-\beta)}{\sqrt{2}\cos\beta}\tilde{h}^d, \\ Y^u_H &= \frac{\cos\alpha}{v\cos\beta}M_u^D + \frac{\sin(\alpha-\beta)}{\sqrt{2}\cos\beta}\tilde{h}^u, \\ Y^d_H &= \frac{\cos\alpha}{v\cos\beta}M_d^D + \frac{\sin(\alpha-\beta)}{\sqrt{2}\cos\beta}\tilde{h}^d, \\ Y^u_A &= -\frac{\tan\beta}{v}M_u^D + \frac{1}{\sqrt{2}\cos\beta}\tilde{h}^u, \\ Y^d_A &= \frac{\tan\beta}{v}M_d^D - \frac{1}{\sqrt{2}\cos\beta}\tilde{h}^d, \\ Y_{1,H^+} &= -\left(\frac{\sqrt{2}\tan\beta}{v}M_u^D - \frac{1}{\cos\beta}(\tilde{h}^u)^\dagger\right)V_{\text{CKM}}, \\ Y_{2,H^+} &= V_{\text{CKM}}\left(\frac{\sqrt{2}\tan\beta}{v}M_d^D - \frac{1}{\cos\beta}\tilde{h}^d\right) \end{aligned} \tag{C.5}$$

with

$$\tilde{h}^u \equiv U_L^\dagger h^u U_R, \quad \tilde{h}^d \equiv D_L^\dagger h^d D_R. \tag{C.6}$$

For $U_L = 1$, we have $\tilde{h}^u = h^u U_R$. As a result,

$$\begin{aligned}
\tilde{h}^u_{31} &= \frac{1}{\sqrt{2}}\frac{v\cos\beta}{m_u}(h^u_{31}(y^u_{11})^* + h^u_{32}(y^u_{12})^*) = 0,\\
\tilde{h}^u_{32} &= \frac{1}{\sqrt{2}}\frac{v\cos\beta}{m_c}(h^u_{31}(y^u_{21})^* + h^u_{32}(y^u_{22})^*) = 0,\\
\tilde{h}^u_{33} &= \frac{1}{\sqrt{2}}\frac{v\sin\beta}{m_t}(|h^u_{31}|^2 + |h^u_{32}|^2)\\
&= \frac{\sqrt{2}m_t}{v\sin\beta}\left(1 - \frac{v^2\cos^2\beta}{2m_t^2}|y^u_{33}|^2\right),
\end{aligned} \tag{C.7}$$

where use is made of Eqs. (3.15), (3.17), and (3.18). Other components of $\tilde{h}^u$ are vanishing. Moreover, with $\tilde{h}^d = V^\dagger_{\rm CKM} h^d$ and using Eq. (3.10) for h^d_{13} and h^d_{23}, we obtain nonzero components of $\tilde{h}^u$ as

$$\begin{aligned}
\tilde{h}^d_{13} &= V^*_{ud}h^d_{13} + V^*_{cd}h^d_{23} = \frac{\sqrt{2}m_b}{v\sin\beta}(V^*_{ud}V_{ub} + V^*_{cd}V_{cb})\\
&= 1.80\times 10^{-2}\left(\frac{m_b}{v\sin\beta}\right),\\
\tilde{h}^d_{23} &= V^*_{us}h^d_{13} + V^*_{cs}h^d_{23} = \frac{\sqrt{2}m_b}{v\sin\beta}(V^*_{us}V_{ub} + V^*_{cs}V_{cb})\\
&= 5.77\times 10^{-2}\left(\frac{m_b}{v\sin\beta}\right),\\
\tilde{h}^d_{33} &= V^*_{ub}h^d_{13} + V^*_{cb}h^d_{23} = \frac{\sqrt{2}m_b}{v\sin\beta}(V^*_{ub}V_{ub} + V^*_{cb}V_{cb})\\
&= 2.41\times 10^{-3}\left(\frac{m_b}{v\sin\beta}\right).
\end{aligned} \tag{C.8}$$

Appendix D: $U(1)'$ interactions

The gauge kinetic terms and mass terms for $U(1)'$ and $U(1)_Y$ are

$$\begin{aligned}
\mathcal{L}_{\rm g.kin} = &-\frac{1}{4}B_{\mu\nu}B^{\mu\nu} - \frac{1}{4}Z'_{\mu\nu}Z'^{\mu\nu} - \frac{1}{2}\sin\xi\, Z'_{\mu\nu}B^{\mu\nu}\\
&-\frac{1}{2}V^T_\mu M^2_V V^\mu,
\end{aligned} \tag{D.1}$$

where $V_\mu = (B_\mu, W^3_\mu, Z'_\mu)^{\rm T}$, and

$$M^2_V = \begin{pmatrix} m^2_Z s^2_W & -m^2_Z c_W s_W & \frac{1}{2}c^{-1}_W e g_{Z'} Q'_{H_2} v^2_2\\ -m^2_Z c_W s_W & m^2_Z c^2_W & -\frac{1}{2}s^{-1}_W e g_{Z'} Q'_{H_2} v^2_2\\ \frac{1}{2}c^{-1}_W e g_{Z'} Q'_{H_2} v^2_2 & -\frac{1}{2}s^{-1}_W e g_{Z'} Q'_{H_2} v^2_2 & m^2_{Z'}\end{pmatrix}. \tag{D.2}$$

After diagonalizing the terms simultaneously with

$$\begin{aligned}
\begin{pmatrix} B_\mu\\ W^3_\mu\\ Z'_\mu\end{pmatrix} &= \begin{pmatrix} c_W & -s_W & -t_\xi\\ s_W & c_W & 0\\ 0 & 0 & 1/c_\xi\end{pmatrix}\begin{pmatrix} 1 & 0 & 0\\ 0 & c_\zeta & s_\zeta\\ 0 & -s_\zeta & c_\zeta\end{pmatrix}\begin{pmatrix} A_\mu\\ Z_{1\mu}\\ Z_{2\mu}\end{pmatrix}\\
&= \begin{pmatrix} c_W & -s_W c_\zeta + t_\xi s_\zeta & -s_W s_\zeta - t_\xi c_\zeta\\ s_W & c_W c_\zeta & c_W s_\zeta\\ 0 & -s_\zeta/c_\xi & c_\zeta/c_\xi\end{pmatrix}\begin{pmatrix} A_\mu\\ Z_{1\mu}\\ Z_{2\mu}\end{pmatrix},
\end{aligned} \tag{D.3}$$

where ζ is the mass mixing angle and $s_W \equiv \sin\theta_W$, $c_W \equiv \cos\theta_W$, etc, we obtain the mass eigenvalues for massive gauge bosons:

$$m^2_{Z_{1,2}} = \frac{1}{2}\left(m^2_Z + m^2_{22} \mp \sqrt{(m^2_Z - m^2_{22})^2 + 4m^4_{12}}\right). \tag{D.4}$$

Here $m^2_Z \equiv (g^2 + g^2_Y)v^2/4$ and

$$\begin{aligned}
m^2_{22} &\equiv m^2_Z s^2_W t^2_\xi + m^2_{Z'}/c^2_\xi - c^{-1}_W e g_{Z'} Q'_{H_2} v^2_w t_\xi/c_\xi,\\
m^2_{12} &\equiv m^2_Z s_W t_\xi - \frac{1}{2}c^{-1}_W s^{-1}_W e g_{Z'} Q'_{H_2} v^2_2/c_\xi.
\end{aligned} \tag{D.5}$$

We can rewrite the Z-boson like mass in terms of the heavy Z' mass and the mixing angle ζ as

$$m^2_{Z_1} = \frac{2m^2_Z\sec 2\zeta + m^2_{Z_2}(1 - \sec 2\zeta)}{1 + \sec 2\zeta}, \tag{D.6}$$

and the mixing angle as

$$\tan 2\zeta = \frac{2m^2_{12}(m^2_{Z_2} - m^2_Z)}{(m^2_{Z_2} - m^2_Z)^2 - m^4_{12}}. \tag{D.7}$$

We note that the modified Z-boson mass is constrained by electroweak precision data, in particular, $\Delta\rho$ or T parameter.

The current interactions including Z' are given by

$$\begin{aligned}
\mathcal{L}_g = B_\mu J^\mu_B + W^3_\mu J^\mu_3 + Z'_\mu J^\mu_{Z'} = &\ A_\mu J^\mu_{\rm EM} + Z_{1\mu}\\
&\times\left(t_\xi s_\zeta c_W J^\mu_{\rm EM} + (c_\zeta - t_\xi s_\zeta s_W)J^\mu_Z - s_\zeta J^\mu_{Z'}/c_\xi\right)\\
&+ Z_{2\mu}\left(-t_\xi c_\zeta c_W J^\mu_{\rm EM} + (s_\zeta - t_\xi c_\zeta s_W)J^\mu_Z + c_\zeta J^\mu_{Z'}/c_\xi\right)
\end{aligned} \tag{D.8}$$

with

$$J^\mu_{\rm EM} = e\bar{f}\gamma^\mu Q_f f,$$
$$J^\mu_Z = \frac{e}{2c_W s_W}\bar{f}\gamma^\mu(\sigma^3 - 2s_W^2 Q_f) f,$$
$$J^\mu_{Z'} = g_{Z'}\bar{f}\gamma^\mu Q'_f f. \tag{D.9}$$

Here Q_f is the electric charge and Q'_f is the $U(1)'$ charge of fermion f. For a small gauge kinetic mixing and/or the mass mixing ζ, the Z'-like gauge boson $Z_{2\mu}$ couples to the electromagnetic current with the overall coefficient of $\varepsilon = t_\xi c_\zeta c_W$.

Ignoring the Z–Z' mixing, the interaction terms for Z' interactions is

$$\begin{aligned}\mathcal{L}_{Z'} = g_{Z'}Z'_\mu\Big(&\frac{1}{3}x\,\bar{t}\gamma^\mu t + \frac{1}{3}x\,\bar{b}\gamma^\mu b + y\bar{\mu}\gamma^\mu\mu \\ &+ y\,\bar{\nu}_\mu\gamma^\mu P_L\nu_\mu - (x+y)\,\bar{\tau}\gamma^\mu\tau \\ &- (x+y)\,\bar{\nu}_\tau\gamma^\mu P_L\nu_\tau + y\,\bar{\nu}_{2R}\gamma^\mu P_R\nu_{2R} \\ &- (x+y)\,\bar{\nu}_{3R}\gamma^\mu P_R\nu_{3R}\Big).\end{aligned} \tag{D.10}$$

Now we change the basis into the one with mass eigenstates by $d_R = D_R d'_R$, $u_R = U_R u'_R$, $d_L = D_L d'_L$ and $u_L = U_L u'_L$ such that $V_{\rm CKM} = U_L^\dagger D_L$. Taking $D_R = U_L = 1$ and $D_L = V_{\rm CKM}$, the above Z' interactions become

$$\begin{aligned}\mathcal{L}_{Z'} = g_{Z'}Z'_\mu\Big(&\frac{1}{3}x\,\bar{t}'\gamma^\mu P_L t' + \frac{1}{3}x\,\frac{v^2\cos^2\beta|y^u_{33}|^2}{2m_t^2}\bar{t}'\gamma^\mu P_R t' \\ &+ \frac{1}{3}x\,\bar{d}'_i\gamma^\mu\Gamma^{dL}_{ij}P_L d'_j + \frac{1}{3}x\,\bar{b}'\gamma^\mu P_R b' \\ &+ y\bar{\mu}\gamma^\mu\mu - (x+y)\,\bar{\tau}\gamma^\mu\tau + y\,\bar{\nu}_\mu\gamma^\mu P_L\nu_\mu \\ &- (x+y)\,\bar{\nu}_\tau\gamma^\mu P_L\nu_\tau \\ &+ y\,\bar{\nu}_{2R}\gamma^\mu P_R\nu_{2R} - (x+y)\,\bar{\nu}_{3R}\gamma^\mu P_R\nu_{3R}\Big),\end{aligned} \tag{D.11}$$

where

$$\begin{aligned}\Gamma^{dL} &\equiv V^\dagger_{\rm CKM}\begin{pmatrix}0&0&0\\0&0&0\\0&0&1\end{pmatrix}V_{\rm CKM} \\ &= \begin{pmatrix}|V_{td}|^2 & V^*_{td}V_{ts} & V^*_{td}V_{tb}\\ V^*_{ts}V_{td} & |V_{ts}|^2 & V^*_{ts}V_{tb}\\ V^*_{tb}V_{td} & V^*_{tb}V_{ts} & |V_{tb}|^2\end{pmatrix}.\end{aligned} \tag{D.12}$$

Considering the general mixing of CP-even scalars while ignoring the Z–Z' mixing, we obtain the interaction between neutral massive electroweak gauge bosons ($V = W, Z$) and Z' as

$$\begin{aligned}\mathcal{L}^{h_i}_V = &\frac{2m_W^2}{v}\left[(\cos\beta R_{i1} + \sin\beta R_{i2})h_i + \frac{1}{2v}h_i^2\right]W_\mu W^\mu \\ &+ \frac{m_Z^2}{v}\left[(\cos\beta R_{i1} + \sin\beta R_{i2})h_i + \frac{1}{2v}h_i^2\right]Z_\mu Z^\mu.\end{aligned} \tag{D.13}$$

For a negligible mixing with the singlet scalar, the above couplings become

$$\begin{aligned}\mathcal{L}^{h/H/A^0}_V = &\frac{2m_W^2}{v}\Big[-\sin(\alpha-\beta)h + \cos(\alpha-\beta)H \\ &+ \frac{1}{2v}(h^2 + H^2 + (A^0)^2)\Big]W_\mu W^\mu \\ &+ \frac{m_Z^2}{v}\Big[-\sin(\alpha-\beta)h + \cos(\alpha-\beta)H \\ &+ \frac{1}{2v}(h^2 + H^2 + (A^0)^2)\Big]Z_\mu Z^\mu.\end{aligned} \tag{D.14}$$

One can see that in the alignment limit with $\alpha = \beta - \pi/2$ the gauge interactions of h are the same as for the SM Higgs while the triple couplings of heavy Higgs boson to gauge bosons vanish.

References

1. R. Aaij et al. [LHCb Collaboration], Phys. Rev. Lett. **113**, 151601 (2014). https://doi.org/10.1103/PhysRevLett.113.151601. arXiv:1406.6482 [hep-ex]
2. S. Bifani, Seminar at CERN (2017). https://indico.cern.ch/event/580620/. Accessed 18 Apr 2017
3. S. Bifani [LHCb Collaboration]. arXiv:1705.02693 [hep-ex]
4. R. Aaij et al. [LHCb Collaboration], JHEP **1708**, 055 (2017). https://doi.org/10.1007/JHEP08(2017)055. arXiv:1705.05802 [hep-ex]
5. R. Aaij et al. [LHCb Collaboration], Phys. Rev. Lett. **111**, 191801 (2013). https://doi.org/10.1103/PhysRevLett.111.191801. arXiv:1308.1707 [hep-ex]
6. R. Aaij et al. [LHCb Collaboration], JHEP **1602**, 104 (2016). https://doi.org/10.1007/JHEP02(2016)104. arXiv:1512.04442 [hep-ex]
7. J.P. Lees et al. [BaBar Collaboration], Phys. Rev. Lett. **109**, 101802 (2012). https://doi.org/10.1103/PhysRevLett.109.101802. arXiv:1205.5442 [hep-ex]
8. J.P. Lees et al. [BaBar Collaboration], Phys. Rev. D **88**(7), 072012 (2013)
9. M. Huschle et al. [Belle Collaboration], Phys. Rev. D **92**(7), 072014 (2015). https://doi.org/10.1103/PhysRevD.92.072014. arXiv:1507.03233 [hep-ex]
10. A. Abdesselam et al. [Belle Collaboration]. arXiv:1603.06711 [hep-ex]
11. R. Aaij et al. [LHCb Collaboration], Phys. Rev. Lett. **115**(11), 111803 (2015) Erratum: [Phys. Rev. Lett. **115** (2015) no.15, 159901] https://doi.org/10.1103/PhysRevLett.115.159901, https://doi.org/10.1103/PhysRevLett.115.111803. arXiv:1506.08614 [hep-ex]

12. L. Bian, S.M. Choi, Y.J. Kang, H.M. Lee, Phys. Rev. D **96**(7), 075038 (2017). https://doi.org/10.1103/PhysRevD.96.075038. arXiv:1707.04811 [hep-ph]
13. H.M. Lee, Phys. Lett. B **778**, 79 (2018). https://doi.org/10.1016/j.physletb.2018.01.010. arXiv:1708.03564 [hep-ph]
14. H. Fritzsch, Z z Xing, S. Zhou, JHEP **1109**, 083 (2011). https://doi.org/10.1007/JHEP09(2011)083. arXiv:1108.4534 [hep-ph]
15. T. Araki, J. Heeck, J. Kubo, JHEP **1207**, 083 (2012). https://doi.org/10.1007/JHEP07(2012)083. arXiv:1203.4951 [hep-ph]
16. A. Crivellin, G. D'Ambrosio, J. Heeck, Phys. Rev. D **91**(7), 075006 (2015). https://doi.org/10.1103/PhysRevD.91.075006. arXiv:1503.03477 [hep-ph]
17. M. Buschmann, J. Kopp, J. Liu, X.P. Wang, JHEP **1606**, 149 (2016). https://doi.org/10.1007/JHEP06(2016)149. arXiv:1601.02616 [hep-ph]
18. W. Altmannshofer, J. Eby, S. Gori, M. Lotito, M. Martone, D. Tuckler, Phys. Rev. D **94**(11), 115032 (2016). https://doi.org/10.1103/PhysRevD.94.115032. arXiv:1610.02398 [hep-ph]
19. A. Crivellin, J. Heeck, D. Mueller. arXiv:1710.04663 [hep-ph]
20. A.W. El Kaffas, W. Khater, O.M. Ogreid, P. Osland, Nucl. Phys. B **775**, 45 (2007). https://doi.org/10.1016/j.nuclphysb.2007.03.041. arXiv:hep-ph/0605142
21. B. Grzadkowski, O.M. Ogreid, P. Osland, Phys. Rev. D **80**, 055013 (2009). https://doi.org/10.1103/PhysRevD.80.055013. arXiv:0904.2173 [hep-ph]
22. A. Drozd, B. Grzadkowski, J.F. Gunion, Y. Jiang, JHEP **1411**, 105 (2014). https://doi.org/10.1007/JHEP11(2014)105. arXiv:1408.2106 [hep-ph]
23. G. Aad et al. [ATLAS Collaboration], Phys. Rev. D **92**(1), 012006 (2015). https://doi.org/10.1103/PhysRevD.92.012006. arXiv:1412.2641 [hep-ex]
24. S. Chatrchyan et al. [CMS Collaboration], JHEP **1401**, 096 (2014). https://doi.org/10.1007/JHEP01(2014)096. arXiv:1312.1129 [hep-ex]
25. G. Aad et al. [ATLAS Collaboration], Phys. Rev. D **91**(1), 012006 (2015). https://doi.org/10.1103/PhysRevD.91.012006. arXiv:1408.5191 [hep-ex]
26. S. Chatrchyan et al. [CMS Collaboration], Phys. Rev. D **89**(9), 092007 (2014). https://doi.org/10.1103/PhysRevD.89.092007. arXiv:1312.5353 [hep-ex]
27. G. Aad et al. [ATLAS Collaboration], Phys. Rev. D **90**(11), 112015 (2014). https://doi.org/10.1103/PhysRevD.90.112015. arXiv:1408.7084 [hep-ex]
28. V. Khachatryan et al. [CMS Collaboration], Eur. Phys. J. C **74**(10), 3076 (2014). https://doi.org/10.1140/epjc/s10052-014-3076-z. arXiv:1407.0558 [hep-ex]
29. G. Aad et al. [ATLAS Collaboration], JHEP **1504**, 117 (2015). https://doi.org/10.1007/JHEP04(2015)117. arXiv:1501.04943 [hep-ex]
30. S. Chatrchyan et al. [CMS Collaboration], JHEP **1405**, 104 (2014). https://doi.org/10.1007/JHEP05(2014)104. arXiv:1401.5041 [hep-ex]
31. G. Aad et al. [ATLAS Collaboration], Eur. Phys. J. C **75**(7), 349 (2015). https://doi.org/10.1140/epjc/s10052-015-3543-1. arXiv:1503.05066 [hep-ex]
32. V. Khachatryan et al. [CMS Collaboration], Eur. Phys. J. C **75**(6), 251 (2015). https://doi.org/10.1140/epjc/s10052-015-3454-1. arXiv:1502.02485 [hep-ex]
33. S. Cassel, D.M. Ghilencea, G.G. Ross, Nucl. Phys. B **827**, 256 (2010). https://doi.org/10.1016/j.nuclphysb.2009.10.029. arXiv:0903.1118 [hep-ph]
34. D.C. Kennedy, B.W. Lynn, Nucl. Phys. B **322**, 1 (1989). https://doi.org/10.1016/0550-3213(89)90483-5
35. B. Capdevila, A. Crivellin, S. Descotes-Genon, J. Matias, J. Virto. arXiv:1704.05340 [hep-ph]
36. W. Altmannshofer, P. Stangl, D.M. Straub, Phys. Rev. D **96**(5), 055008 (2017). https://doi.org/10.1103/PhysRevD.96.055008. arXiv:1704.05435 [hep-ph]
37. L.S. Geng, B. Grinstein, S. Jger, J. Martin Camalich, X.L. Ren, R.X. Shi, Phys. Rev. D **96**(9), 093006 (2017). https://doi.org/10.1103/PhysRevD.96.093006. arXiv:1704.05446 [hep-ph]
38. M. Ciuchini, A.M. Coutinho, M. Fedele, E. Franco, A. Paul, L. Silvestrini, M. Valli, Eur. Phys. J. C **77**(10), 688 (2017). https://doi.org/10.1140/epjc/s10052-017-5270-2. arXiv:1704.05447 [hep-ph]
39. D. Ghosh, Eur. Phys. J. C **77**(10), 694 (2017). https://doi.org/10.1140/epjc/s10052-017-5282-y. arXiv:1704.06240 [hep-ph]
40. A.K. Alok, B. Bhattacharya, A. Datta, D. Kumar, J. Kumar, D. London, Phys. Rev. D **96**(9), 095009 (2017). https://doi.org/10.1103/PhysRevD.96.095009. arXiv:1704.07397 [hep-ph]
41. D. Bardhan, P. Byakti, D. Ghosh, Phys. Lett. B **773**, 505 (2017). https://doi.org/10.1016/j.physletb.2017.08.062. arXiv:1705.09305 [hep-ph]
42. A. Crivellin, A. Kokulu, C. Greub, Phys. Rev. D **87**(9), 094031 (2013). https://doi.org/10.1103/PhysRevD.87.094031. arXiv:1303.5877 [hep-ph]
43. A. Faessler, T. Gutsche, S. Kovalenko, V.E. Lyubovitskij, I. Schmidt, Phys. Rev. D **82**, 075012 (2010). https://doi.org/10.1103/PhysRevD.82.075012. arXiv:1007.2496 [hep-ph]
44. B. Bhattacharya, A. Datta, J.P. Guvin, D. London, R. Watanabe, JHEP **1701**, 015 (2017). https://doi.org/10.1007/JHEP01(2017)015. arXiv:1609.09078 [hep-ph]
45. Y. Amhis et al. [Heavy Flavor Averaging Group (HFAG)]. arXiv:1412.7515 [hep-ex]
46. L. Di Luzio, M. Kirk, A. Lenz. arXiv:1712.06572 [hep-ph]
47. P. Ko, Y. Omura, Y. Shigekami, C. Yu, Phys. Rev. D **95**(11), 115040 (2017). https://doi.org/10.1103/PhysRevD.95.115040. arXiv:1702.08666 [hep-ph]
48. F. Borzumati, C. Greub, Phys. Rev. D **58**, 074004 (1998). https://doi.org/10.1103/PhysRevD.58.074004. arXiv:hep-ph/9802391
49. M. Misiak et al., Phys. Rev. Lett. **114**(22), 221801 (2015). https://doi.org/10.1103/PhysRevLett.114.221801. arXiv:1503.01789 [hep-ph]
50. M. Czakon, P. Fiedler, T. Huber, M. Misiak, T. Schutzmeier, M. Steinhauser, JHEP **1504**, 168 (2015). https://doi.org/10.1007/JHEP04(2015)168. arXiv:1503.01791 [hep-ph]
51. A. Paul, D.M. Straub, JHEP **1704**, 027 (2017). https://doi.org/10.1007/JHEP04(2017)027. arXiv:1608.02556 [hep-ph]
52. S. Fajfer, J.F. Kamenik, I. Nisandzic, Phys. Rev. D **85**, 094025 (2012). https://doi.org/10.1103/PhysRevD.85.094025. arXiv:1203.2654 [hep-ph]
53. A. Crivellin, C. Greub, A. Kokulu, Phys. Rev. D **86**, 054014 (2012). https://doi.org/10.1103/PhysRevD.86.054014. arXiv:1206.2634 [hep-ph]
54. A. Djouadi, Phys. Rep. **457**, 1 (2008). https://doi.org/10.1016/j.physrep.2007.10.004. arXiv:hep-ph/0503172
55. R.D. Ball et al., Nucl. Phys. B **867**, 244 (2013). https://doi.org/10.1016/j.nuclphysb.2012.10.003. arXiv:1207.1303 [hep-ph]
56. A. Buckley, J. Ferrando, S. Lloyd, K. Nordstrm, B. Page, M. Rfenacht, M. Schnherr, G. Watt, Eur. Phys. J. C **75**, 132 (2015). https://doi.org/10.1140/epjc/s10052-015-3318-8. arXiv:1412.7420 [hep-ph]
57. S. von Buddenbrock et al., Eur. Phys. J. C **76**(10), 580 (2016). https://doi.org/10.1140/epjc/s10052-016-4435-8. arXiv:1606.01674 [hep-ph]
58. S. von Buddenbrock, A.S. Cornell, A. Fadol, M. Kumar, B. Mellado, X. Ruan. arXiv:1711.07874 [hep-ph]
59. V. Khachatryan et al. [CMS Collaboration], Phys. Rev. Lett. **117**(3), 031802 (2016). https://doi.org/10.1103/PhysRevLett.117.031802. arXiv:1604.08907 [hep-ex]
60. ATLAS Collaboration, ATLAS-CONF-2016-030

61. CMS Collaboration, CMS-PAS-EXO-16-030
62. The ATLAS collaboration [ATLAS Collaboration], ATLAS-CONF-2016-029
63. The ATLAS collaboration [ATLAS Collaboration], ATLAS-CONF-2016-070
64. V. Khachatryan et al. [CMS Collaboration], Phys. Lett. B **749**, 560 (2015). https://doi.org/10.1016/j.physletb.2015.08.047. arXiv:1503.04114 [hep-ex]
65. V. Khachatryan et al. [CMS Collaboration], Eur. Phys. J. C **76**(7), 371 (2016). https://doi.org/10.1140/epjc/s10052-016-4206-6. arXiv:1602.08762 [hep-ex]
66. G. Aad et al. [ATLAS Collaboration], Eur. Phys. J. C **75**(9), 412 (2015). https://doi.org/10.1140/epjc/s10052-015-3628-x. arXiv:1506.00285 [hep-ex]
67. M. Aaboud et al. [ATLAS Collaboration], Phys. Rev. D **94**(5), 052002 (2016). https://doi.org/10.1103/PhysRevD.94.052002. arXiv:1606.04782 [hep-ex]
68. V. Khachatryan et al. [CMS Collaboration], JHEP **1602**, 145 (2016). https://doi.org/10.1007/JHEP02(2016)145. arXiv:1506.01443 [hep-ex]
69. CMS Collaboration [CMS Collaboration], CMS-PAS-B2G-16-003
70. M. Aaboud et al. [ATLAS Collaboration], Phys. Lett. B **765**, 32 (2017). https://doi.org/10.1016/j.physletb.2016.11.045. arXiv:1607.05621 [hep-ex]
71. V. Khachatryan et al. [CMS Collaboration], JHEP **1511**, 018 (2015). https://doi.org/10.1007/JHEP11(2015)018. arXiv:1508.07774 [hep-ex]
72. G. Aad et al. [ATLAS Collaboration], JHEP **1603**, 127 (2016). https://doi.org/10.1007/JHEP03(2016)127. arXiv:1512.03704 [hep-ex]
73. A.G. Akeroyd, A. Arhrib, E.M. Naimi, Phys. Lett. B **490**, 119 (2000). https://doi.org/10.1016/S0370-2693(00)00962-X. arXiv:hep-ph/0006035
74. I.F. Ginzburg, I.P. Ivanov, Phys. Rev. D **72**, 115010 (2005). https://doi.org/10.1103/PhysRevD.72.115010. arXiv:hep-ph/0508020
75. S. Kanemura, K. Yagyu, Phys. Lett. B **751**, 289 (2015). https://doi.org/10.1016/j.physletb.2015.10.047. arXiv:1509.06060 [hep-ph]